«ФИЗИКА ЭЛЕМЕНТАРНЫХ ЧАСТИЦ И АТОМНОГО ЯДРА»
1992, ТОМ 23, ВЫП.4

УДК 539.149

MICROSCOPIC DESCRIPTION OF THE SHAPE COEXISTENCE IN THE A ~ 70 MASS REGION

A.Petrovici [1,2,3], *K.W.Schmid* [2], *A.Faessler*[2]

The shape coexistence phenomena dominating the structure of the nuclei in the $A \sim 70$ mass region are investigated within different approaches using general symmetry-projected Hartree — Fock — Bogolubov configurations as basic building blocks, a rather large model space, and a suitably defined effective two-body interaction. The selection of the relevant configurations is let to the dynamics of the considered system in the frame of the EXCITED VAMPIR and EXCITED FED VAMPIR variational procedures involving *real* or *complex* mean fields. The results concerning the structure of low and high spin states in a couple of even-even Ge, Se, and Kr nuclei indicate that a variable mixing of more or less deformed prolate and oblate quasiparticle determinants is responsible for the complex behaviour of the doubly-even nuclei in this mass region.

Явление сосуществования форм, являющееся определяющим для структуры ядер с $A \sim 70$, исследовано в рамках различных подходов, использующих в качестве базиса проектированные волновые функции метода Хартри — Фока — Боголюбова, большое пространство состояний и соответствующим образом подобранное эффективное двухчастичное взаимодействие. Отбор существенных конфигураций определяет динамику рассматриваемых систем, исследуемую в рамках EXCITED VAMPIR и EXCITED FED VAMPIR вариационных процедур, включающих вещественное или комплексное среднее поле. Результаты, относящиеся к структуре низко- и высокоспиновых состояний в ряде четно-четных изотопов Ge, Se и Kr, показывают, что изменяющееся смешивание квазичастичных детерминантов, соответствующих более-менее деформированным вытянутой и сплюснутой формам, ответственно за сложное поведение четно-четных ядер в исследуемой массовой области.

1. INTRODUCTION

Studies of nuclei far from stability revealed an unexpected variety of nuclear structures and motions which are challenging and improving continuously our understanding of a nucleus. The experimental

[1]Institute for Physics and Nuclear Engineering, Bucharest, Romania
[2]Institut für Theoretische Physik, Universität Tübingen, D-7400 Tübingen, Germany
[3]Department of Physics, University of Jyväskylä, SF-40100 Jyväskylä, Finland

investigations progressed with the development of acceleration techniques, improvement of isotope separation, advances in instrumentation and new detection methods. On the other hand, the new experimental information concerning low- and high-spin spectra, electromagnetic properties of short-lived states and also inelastic electron scattering data gave a challenge to theoretical nuclear structure physics and led to a rapid development of rather successful theoretical methods.

Particular attention has been paid to the nuclei belonging to the $A \sim 70$ mass region. According to both the experimental systematics and the theoretical calculations, the mass $A \sim 70$ nuclei have a transitional character and display a rich pattern of shape coexistence and shape transition. The multiplicity of structures, the rapid and also drastic changes of the properties with the number of nucleons and the interplay of collective and single-particle motions make the $A = 70$—80 region an important testing ground of nuclear models [1]. Unfortunately, a microscopic insight into the shape coexistence phenomena dominating the structure of the mass 70 region by a complete diagonalization of a suitably chosen effective many-nucleon Hamiltonian, as it is done in the Shell-model Configuration Mixing (SCM) approach, is severely hindered, because a large number of valence nucleons are distributed among many single particle levels. Therefore the theoretical studies [2—11] which tried to explain the interesting behaviour of doubly-even nuclei around mass number $A \sim 70$ have been carried out either in rather restricted configuration spaces in the frame of the usual shell model or using several collective models or models involving an interplay of particles and collective excitations. A clear understanding of all the known facts was not possible.

The even-even nuclei of the $A \sim 70$ region display a couple of interesting features which are rather unique in the nuclear mass table (see, e.g., ref. [1] and references therein). The coexistence of overlapping bands built on different nuclear shapes, and also the observation of many low spin states, e.g., 0^+ or 2^+ states, at very low excitation energy, is related to the competition between various large gaps at different deformations displayed by the Nilsson single particle energy diagrams. Furthermore, the nuclei in this mass region have usually both active protons and neutrons in the $0g_{9/2}$ shell-model orbit. Since there are many different ways to couple these particles to intermediate and high-spin values, a competition of many configurations at these spin values is rather likely, too.

For a deeper theoretical understanding of the complex experimental situation encountered in the mass $A \sim 70$ nuclei, one needs a microscopic model in which all the essential degrees of freedom of collective as well as single particle nature are not put in by hand but accounted for in a completely

microscopic fashion. For this purpose we use here the variational techniques developed for various models of the so-called VAMPIR (Variation After Mean Field Projection In Realistic model spaces) family [12]. The two most sophisticated procedures out of this family, which has been continuously extended and improved during the last couple of years, are the EXCITED VAMPIR and EXCITED FED VAMPIR approximations. As we shall see these are rather adequate to describe the shape coexistence phenomena.

The EXCITED VAMPIR model is essentially a mean field theory which solves the Hartree — Fock — Bogolubov problem with spin and number projection before the variation for yrast and nonyrast states. In this approximation an optimized mean field is obtained for each state of a given symmetry by a chain of independent variational calculations and, finally, the residual interaction in the resulting A-nucleon configuration space is diagonalized. Our first investigations concerned the low spin excitation spectra for a couple of doubly-even Ge as well as Se isotopes [13] in the frame of the EXCITED VAMPIR model based on *real* HFB transformations. We found that a variable mixing of more or less deformed prolate and oblate projected quasiparticle determinants is able to produce the experimental picture for the low-spin states of the considered Ge and Se isotopes, like the presence of 4—5 coexisting 0^+ or 2^+ states below 3—4 MeV excitation energy, as well as the general trends in the quadrupole moments, $B(E0)$ and $B(E2)$ values, and the proton and neutron occupations of the spherical single particle orbitals. These results strongly supported the shape coexistence as a dominant feature of the low spin states in even Ge and Se nuclei.

Encouraged by this success the *real* EXCITED VAMPIR investigations were extended to the high-spin states in the ^{68}Ge, ^{70}Se and ^{72}Se nuclei [14]. It turned out that the shape coexistence persists and manifests specifically at high-spin states. A strong bunching of states of a given spin and parity in a small excitation energy interval was predicted as well as a variable, sometimes very strong, mixing in between these states which creates a complex feeding pattern for the yrast band, including competing $M1$, $\Delta I = 0$ transitions. Nevertheless, the high-spin states could still be grouped into bands based on different structures, some of them connected by $E2$ crossing transitions.

In order to understand how reliable the EXCITED VAMPIR description of the considered states really was, an improvement of the theoretical approximation was necessary. This was achieved by the so-called EXCITED FED (from FEw Determinants) VAMPIR method [15,16] which goes beyond the symmetry projected quasiparticle mean field approximation. In this approach each state is described not by only one determinant, but by a linear combination of a few projected determinants obtained successively in a chain of variational calculations, asking in each step for maximum residual interaction and by this for maximum additional contribution to that state.

By this procedure the remaining residual interaction between the resulting few lowest states of a given symmetry becomes much smaller than in the case of the uncorrelated EXCITED VAMPIR solutions, and thus the reliability of the wave functions is increased considerably. The nature of each high-spin band is more precisely distinguished since the dominant correlations for each particular configuration are included in a systematic way. Reinvestigating the low- and high-spin states of ^{68}Ge with this new method we found that the qualitative features of the EXCITED VAMPIR description persist. It was also possible to identify out of the many overlapping bands one having considerably larger deformation, $\beta_2 \sim 0.42$, than the other bands in ^{68}Ge and in other Ge nuclei. This is a strikingly large deformation for such a light nucleus, however, as we shall see, recent experimental data confirm this prediction [17].

A more quantitative confirmation of the rather complicated theoretical picture of the structure of the nuclei in the $A \sim 70$ mass region comes from the comparison of the charge and transition charge densities in several even Ge isotopes [18] with the available data extracted from elastic and inelastic electron scattering [19].

Quantitative changes of the complex picture emerging from these studies which are only based on *real* Hartree — Fock — Bogolubov transformations had to be expected when we included unnatural parity pairing correlations by essentially *complex* mean fields. However, the qualitative features of the complex behaviour of the nuclei in this mass region persist even in such more refined calculations as indicate the first results which we obtained very recently within the *complex* versions of the VAMPIR models [23].

In this review only selected highlights will be presented, which will include: the basic ideas behind the microscopic approaches used in our theoretical investigations; the *real* EXCITED VAMPIR picture concerning the coexistence of multiple shapes and structures associated with quite different deformations in a couple of even Ge and Se isotopes at low excitations; some new aspects of the nuclear shape coexistence in the $A \sim 70$ mass region obtained going beyond symmetry-projected quasiparticle mean fields; new insights into the structure of $N = Z$ nuclei gained using complex mean fields. These new results may illustrate the power of the continuously developing realistic microscopic approaches belonging to the VAMPIR model family.

2. THE THEORETICAL FRAMEWORK

In this section we shall briefly sketch the EXCITED VAMPIR and EXCITED FED VAMPIR approximations, the most sophisticated variational procedures of the VAMPIR model family, where the construction of the

configuration space itself is entirely left to the dynamics of the considered system and determined by a chain of successive variational calculations. Also we shall discuss the basic assumptions and ingredients of the models as well as to the model space and the effective interaction.

2.1. Basic Assumptions and Ingredients of the Theory. We restrict ourselves to the investigation of the structure of the nuclear ground state and low lying discrete excitations at «low excitation energy and momentum transfer». Therefore we assume that it is possible to use an effective two-body interaction in a finite model space. The effective many-nucleon Hamiltonian appropriate for a finite model space in a given mass region consisting of general one- and two-body terms is assumed to be given by:

$$\hat{H} = \sum_{i,k=1}^{M} t\,(ik) c_i^\dagger c_k + \frac{1}{4} \sum_{i,k,r,s=1}^{M} v\,(ikrs) c_i^\dagger c_k^\dagger c_s c_r\,, \tag{2.1}$$

where $t\,(ik) \equiv \langle i \mid \hat{t} \mid k \rangle$ are the matrix elements of the one-body operator of the kinetic energy (or, if an inert core is used, some suitably chosen single particle energies) and $v\,(ikrs) \equiv \langle ik \mid \hat{v} \mid rs - sr \rangle$ are the antisymmetrized matrix elements of the effective two-body interaction. The Hamiltonian is represented in terms of creation $\{c_i^\dagger, c_k^\dagger, \ldots\}_M$ and annihilation $\{c_i, c_k, \ldots\}_M$ fermion operators corresponding to our model space defined by a finite, M-dimensional set $\{|i\rangle, |k\rangle, \ldots\}_M$ of orthonormal single nucleon states, e.g., harmonic oscillator wave functions.

The truncation schemes which we use to get the best approximations to the in large model spaces inaccessible «exact» solutions are based on the Hartree — Fock — Bogolubov (HFB) theory.

The first step to the ansatz of our many-body wave function is to define the quasi-particle creators and annihilators via

$$a_\alpha^\dagger \equiv \sum_{i=1}^{M} (A_{i\alpha}\, c_i^\dagger + B_{i\alpha}\, c_i), \tag{2.2}$$

$$a_\alpha \equiv \sum_{i=1}^{M} (B_{i\alpha}^*\, c_i^\dagger + A_{i\alpha}^*\, c_i). \tag{2.3}$$

In matrix notation these equations can be combined to

$$\begin{pmatrix} a^\dagger \\ a \end{pmatrix} = \begin{pmatrix} A^T & B^T \\ B^\dagger & A^\dagger \end{pmatrix} \begin{pmatrix} c^\dagger \\ c \end{pmatrix} \equiv F \begin{pmatrix} c^\dagger \\ c \end{pmatrix} \tag{2.4}$$

with F being a unitary $(2M \times 2M)$-dimensional matrix.

The corresponding HFB-vacuum is defined by $a_\alpha \mid F> \equiv 0$ for all $\alpha = 1,...,M$ and may be represented as

$$\mid F> = \left(\prod_{\alpha=1}^{M'} a_\alpha \right) \mid 0> \quad \text{with} \quad M' \leq M. \tag{2.5}$$

Since the transformation (2.4) sums over all the quantum numbers characterizing the single particle basis states, $\mid F>$ violates angular momentum, particle number and charge conservation and, in general, has no definite parity either. In order to obtain the physical configurations we have to restore the broken symmetries.

From the vacuum (2.5) configurations with the desired symmetry quantum numbers $s \equiv AT_z I^\pi$ can be constructed using the operator

$$\hat{\Theta}^s_{MK} \equiv \hat{P}\,(IM; K)\,\hat{Q}\,(2T_z)\,\hat{Q}\,(A)\,\hat{p}\,(\pi). \tag{2.6}$$

Here

$$\hat{p}\,(\pi) \equiv \frac{1}{2}\,(1 + \pi\,\hat{\Pi}), \tag{2.7}$$

with $\hat{\Pi}$ being the parity operator projects onto definite parity π.

$$\hat{Q}(A) \equiv \frac{1}{2\pi} \int_0^{2\pi} d\varphi \exp\{i\varphi\,(A - \hat{A})\}, \tag{2.8}$$

with $\hat{A}$ being the nucleon number operator, restores the desired total nucleon number A, and

$$\hat{Q}\,(2T_z) \equiv \frac{1}{2\pi} \int_0^{2\pi} d\chi \exp\{i\chi\,(N - Z - \hat{N} + \hat{Z})\}, \tag{2.9}$$

with $\hat{N}$ and $\hat{Z}$ being the neutron and the proton number operators, respectively, selects the components with a definite total isospin projection $2T_z = N - Z$. Finally

$$\hat{P}\,(IM; K) \equiv \frac{2I + 1}{8\pi^2} \int_0^{4\pi} d\Omega\, D^{I^*}_{MK}\,(\Omega)\,\hat{R}\,(\Omega), \tag{2.10}$$

with $\hat{R}\,(\Omega)$ being the usual rotation operator and $D^I_{MK}\,(\Omega)$ denoting its representation in angular momentum eigenstates, constructs from the $I_3 = K$ component in the symmetry-breaking «intrinsic» frame of reference a configuration in the laboratory frame with total angular momentum I and 3-

component $I_z = M$. The unphysical dependence on the orientation of the intrinsic quantization axis can be eliminated by taking linear combinations of the form

$$|\phi_\rho; sM> \equiv \sum_{K=-I}^{I} \hat{\Theta}^s_{MK} |F>_{f_{K;\rho}} . \tag{2.11}$$

In order to simplify the numerics up to about two years ago a couple of symmetry restrictions had been imposed on the general HFB transformation F: time-reversal and axial symmetry had been required, parity- as well as proton-neutron mixing being neglected, and last but not least only real transformations F had been admitted.

According to the Bloch and Messiah [20] the HFB vacuum (2.5) then gets the canonical form

$$|F> = \prod_{r=p,n} \left\{ \prod_{\pi=+,-} \left[\prod_{m=1/2}^{m_{\max}} \left(\prod_{\alpha}^{(\tau,\pi,m)} [u_\alpha + v_\alpha b^\dagger_\alpha \hat{b}^\dagger_\alpha] \right) \right] \right\} |0>, \tag{2.12}$$

where

$$b^\dagger_\alpha \equiv \hat{\tau} b^\dagger_\alpha \hat{\tau}^{-1}, \tag{2.13}$$

with $\hat{\tau}$ being the time-reversal operator, and u_α and v_α are all real numbers with $u_\alpha \geq 0$ and $u^2_\alpha + v^2_\alpha = 1$ for all α.

The basic «building block» of the symmetry-restricted vacuum (2.12) can be represented as

$$b^\dagger_\alpha \hat{b}^\dagger_\alpha = \sum_{i \leq k}^{(m_\alpha \tau_\alpha \pi_\alpha)} [1 + \delta(i,k)]^{-1} \sum_I (-)^{j_k + l_k - m_\alpha} (j_i j_k I | m_\alpha - m_\alpha 0) \times$$

$$\times \left\{ D_{i\alpha} D_{k\alpha} [1 + (-)^I] [c^\dagger_i c^\dagger_k]^{I0}_{12\tau_\alpha} \right\}, \tag{2.14}$$

where D is the corresponding *real* first Bloch — Messiah transformation, which mixes in this case only states with the same m, τ, π quantum numbers, i denotes the triple of quantum numbers n_i, l_i, j_i of the basis state and the creators of the coupled two-nucleon states are given by

$$[c^\dagger_i c^\dagger_k]^{IM}_{TT_z} = \sum_{m_i m_k \tau_i \tau_k} (j_i j_k I | m_i m_k M) \left(\tfrac{1}{2}\tfrac{1}{2} T | \tau_i \tau_k T_z\right) c^\dagger_i c^\dagger_k \tag{2.15}$$

Thus the basic building-block and hence the total vacuum, too, contains only «like»-nucleon pairs coupled to even angular momenta and positive parity. Therefore using the mentioned symmetry restrictions we can

investigate only states with even angular momentum and positive parity in doubly even nuclei. However, we shall see in sections 3 and 4 that we can go rather far even with this symmetry restricted *real* HFB transformations. Recently [15,22,23] we have succeeded in improving the approaches on the lines proposed in ref. [21] taking into account parity- as well as proton-neutron mixing and admitting essentially *complex* mean fields. Only time-reversal invariance and axial symmetry are kept. Consequently the now *complex* first Bloch — Messiah transformation D mixes all quantum numbers except m. It gets the form

$$b_\alpha^\dagger \equiv \sum_{i=1}^{M} \delta(m_i, m_\alpha)\, D_{i\alpha}^*\, c_i^\dagger\,; \quad m_\alpha > 0 \tag{2.16}$$

and

$$b_{\bar{\alpha}}^\dagger \equiv \sum_{i=1}^{M} \delta(m_i, m_\alpha)\, D_{i\alpha}\, c_{\bar{i}}^\dagger\,; \quad m_\alpha > 0. \tag{2.17}$$

The corresponding «canonical» HFB vacuum takes the form

$$|F> = \left\{ \prod_{m=1/2}^{m_{\max}} \left(\prod_{\alpha}^{(m)} [u_\alpha + v_\alpha\, b_\alpha^\dagger\, b_{\bar{\alpha}}^\dagger] \right) \right\} |0>, \tag{2.18}$$

and its basic building block can be written as

$$\begin{aligned} b_\alpha^\dagger\, b_{\bar{\alpha}}^\dagger = {} & \sum_{\tau=p,n} \sum_{\mathrm{i} \le \mathrm{k}}^{(m_\alpha \tau)} \left[1 + \delta(\mathrm{i},\mathrm{k})\right]^{-1} \sum_I (-)^{j_k + l_k - m_\alpha} (j_i\, j_k\, I \,|\, m_\alpha - m_\alpha 0) \times \\ & \times \left\{ \left[\mathrm{Re}(D_{i_\tau \alpha}^* D_{k_\tau \alpha}) [1 + (-)^{l_i + l_k + I}] + i\, \mathrm{Im}(D_{i_\tau \alpha}^* D_{k_\tau \alpha}) [1 - (-)^{l_i + l_k + I}] \right] [c_i^\dagger c_k^\dagger]_{12\tau}^{I0} \right\} + \\ & + \sum_{\mathrm{i}}^{(m_\alpha p)} \sum_{\mathrm{k}}^{(m_\alpha n)} \sum_{IT} (1/21/2T \,|\, -1/21/20)\, (-)^{j_k + l_k - m_\alpha} (j_i\, j_k\, I \,|\, m_\alpha - m_\alpha 0) \times \\ & \times \left\{ \left[\mathrm{Re}(D_{i_p \alpha}^* D_{k_n \alpha}) [1 + (-)^{l_i + l_k + I}] + i\, \mathrm{Im}(D_{i_p \alpha}^* D_{k_n \alpha}) [1 - (-)^{l_i + l_k + I}] \right] [c_i^\dagger c_k^\dagger]_{T0}^{I0} \right\}. \end{aligned} \tag{2.19}$$

It contains all possible two-nucleon couplings including pairing correlations between like-nucleons as well as both the $T = 0$ and the $T = 1$ pairing correlations between protons and neutrons. Now states with arbitrary parity and angular momentum in both doubly even and doubly odd systems can be described.

With the basic ingrediences of the theory being introduced, we shall now briefly review the variational procedures which have been used to investigate some even-even nuclei in the $A \sim 70$ mass region.

2.2. Variational Procedures. Let us first assume that we are interested in the yrast state of a particular symmetry $s \equiv AT_z I^\pi$, e.g., the lowest $I^\pi = 8^+$ state in some even mass nucleus. In this case one starts with a general HFB vacuum projected onto the desired symmetry quantum numbers as trial wave function and extracts the underlying quasiparticle transformation via a variational calculation directly from the chosen effective many-body Hamiltonian. Minimizing the corresponding energy-functional

$$E_1^s[F_1^s] = \frac{<\phi_1;\, sM \mid \hat{H} \mid \phi_1;\, sM>}{<\phi_1;\, sM \mid \phi_1;\, sM>} \tag{2.20}$$

with respect to arbitrary variations of the HFB transformation F_1^s, one obtains the optimal approximation to this state which can be reached by a single symmetry-projected HFB determinant. This is the VAMPIR [12] approach to this particular yrast state. Note, that because of the symmetry projection before the variation the resulting transformation depends on the symmetry. Thus, already in this simplest approach, e.g., drastic changes of the structure with increasing spin can be described. The extension for the description of the excited states with the same symmetry is the EXCITED VAMPIR approach [12—14]. In this approximation excited states with the same symmetry, e.g., the first excited $I^\pi = 8^+$ state, are calculated in complete analogy, with the only difference that one has to ensure the orthogonality of the current trial wave function with respect to the VAMPIR solution. In other words, one eliminates the lowest solution for the considered symmetry from the variational space by Gram — Schmidt orthogonalization and then calculates the optimal approximation to the first excited state which can be reached again by a single symmetry-projected HFB determinant. If the first excited state is obtained, it is eliminated, too, and then the second excited state is calculated, and so on, up to m different symmetry-projected HFB determinants, optimal for the m lowest states of the considered symmetry, have been constructed.

Therefore we use as test wave function for the n-th state ($n > 0$) of a given symmetry the following ansatz

$$\mid \varphi_n;\, sM> \sim \sum_{i=1}^{n} \mid \phi_i;\, sM> \beta_i^n = \sum_{i=1}^{n} \hat{\Theta}_{M0}^s \mid F_i^s> \beta_i^n, \tag{2.21}$$

with the β_i^n given by requiring normalization and orthogonality with respect to all the $(n-1)$ solutions already obtained and $|F_n^s>$ being left free for the variation. Note, that the variational calculation for each new determinant is completely independent of the one performed for any of the previous states with the same symmetry. Finally the residual interaction in this basis of orthonormal A-nucleon configurations with the symmetry s is diagonalized and the final EXCITED VAMPIR wave functions are obtained

$$|\Psi_\alpha^{(m)}; sM> = \sum_{i=1}^{m} |\varphi_i; sM> g_{i;\alpha}^{(m)s}. \tag{2.22}$$

However, using only one additional determinant for each new state to be considered this approach is still a sort of mean field approximation and may not always be sufficient, since the residual interaction between the m lowest configurations does not necessarily account for the dominant correlations on the top of each of the various EXCITED VAMPIR solutions. It may very well be that the dominant correlations to a main mean field for a given state are due to rather high lying configurations, or due to configurations which have a completely different structure than those underlying the lowest m orthogonal A-nucleon solutions for a given symmetry.

An improved variational scheme incorporating such correlations in a systematic way, no matter where in energy they occur, the EXCITED FED VAMPIR approach [15,16,18], allows one to go beyond mean fields. The variational procedure performs as follows: for the yrast state of a given symmetry one starts again with the VAMPIR solution. Now one looks for a second symmetry-projected determinant correlating this solution, but the main one is not taken out of the variational space. This is again obtained by a variational calculation so that always that configuration is found which yields the maximal additional energy for the considered yrast solution. After that a third determinant is constructed, etc., up to altogether n_1 configurations have been obtained. The resulting correlated yrast state is then eliminated from the variational space, and the procedure is repeated for the first excited state with the same symmetry, and so on, up to finally the m lowest states have been constructed. Thus in this approximation the i-th state of a given symmetry is represented as a linear combination of few projected quasiparticle determinants constructed successively in a chain of variational calculations, the state being Schmidt orthogonalized with respect to all the $i-1$ already found solutions. In each step of the variational chain for the i-th «correlated» wave function one varies only the last added mean field and the configuration mixing coefficients which ensures the orthonormality of the resulting linear independent solutions, asking for maximum additional con-

tribution to the energy of the previous approximation to that wave function. Such a properly normalized linear combination of n_i different HFB-type determinants $|F_k\rangle$ $(k = i,..,n_i)$ is created for the i-th state of symmetry s

$$|\Phi_i^{(n_i)}; sM\rangle \equiv \hat{T}^{(i)} \hat{\Theta}^s_{M0} \sum_{\nu=1}^{n_i} |F_{q+\nu}\rangle f^{in_i}_{\nu;1}$$
$$\equiv \hat{\Theta}^s_{M0} \sum_{j=1}^{\omega(i)} |F_j\rangle \eta^i_{j;1}, \tag{2.23}$$

where $\hat{T}^{(i)}$ eliminates the first $i-1$ solutions from the model space with q indicating the total number of building determinants, $q \equiv \sum_{j=1}^{i-1} n_j$, and $\omega(i) \equiv \sum_{i=1}^{i} n_i$. Finally as already in the EXCITED VAMPIR approximation, the residual interaction between the m energetically lowest linear combinations is diagonalized and the lowest m physical states of symmetry s

$$|\Psi_\alpha^{(m)}; sM\rangle = \sum_{i=1}^{m} |\Phi_i^{(n_i)}; sM\rangle g^{(m)}_{i\alpha}, \quad \alpha = 1,...,m \tag{2.24}$$

and the corresponding energies $E^{(m)}_\alpha$ $(\alpha = 1,...,m)$ are obtained

$$(H - E^{(m)}1)\, g^{(m)} = 0$$
$$g^{(m)\dagger}\, g^{(m)} = 1_m. \tag{2.25}$$

The EXCITED FED VAMPIR variational procedure, going beyond the symmetry-projected quasiparticle mean field approximations, automatically selects the relevant degrees of freedom for the main mean field underlying the structure of a particular state, and also accounts for the most important additional correlations with respect to the approximation already obtained. In this way arbitrary drastic changes of the structure with increasing excitation energy or spin are accessible and furthermore various types of shape coexistence could be distinguished. The particular mentioned features of this model are essential for an adequate description of the structure of nuclei displaying a dynamical shape coexistence. The improvement with respect to the EXCITED VAMPIR approximation comes from the fact that the dominant correlations on top of the optimal projected mean field solutions are incorporated for each state separately. In this way each of the still neglected configurations could bring to the energy for the already obtained states only gains comparable with that from the last correlating configuration included for any of them. Also the residual interaction will be at most at this level and

of course much smaller and by that, the confidence level of the resulting wave functions is improved.

Of course, the *complex* versions of the VAMPIR, EXCITED VAMPIR, FED VAMPIR and EXCITED FED VAMPIR approaches (later on referred to as CV, CEV, CFV and CEFV, respectively) represent a remarkable improvement with respect to their *real* restricted partners (RV, REV, RFV and REFV). This will be exemplified below by recently obtained results concerning new aspects of the shape coexistence at low excitation energies in an even-even $N = Z$ system.

2.3. The Model Space and the Effective Interaction. Calculations in the $A \sim 70$ region within the *real* versions of the EXCITED VAMPIR and EXCITED FED VAMPIR approximations have been performed using a rather large model space: the full $N = 3$ and $N = 4$ shells for both protons and neutrons and for the latter in addition the $0h_{11/2}$ orbital. As effective two-body interaction a Brueckner nuclear matter G-matrix derived from the Bonn-OBEP [24] had been taken, which was renormalized by adding two short-range (0.7 fm) Gaussians with strengths of −50 MeV and −40 MeV to the $T = 1$ proton-proton and neutron-neutron relative matrix-elements, respectively, introduced to enhance the pairing components. An isospin-independent spin-orbit Gaussian was added, and, finally the onset of deformation was influenced by a monopole shift in all the diagonal $T = 0$ matrix elements of the form $<0g_{9/2}0f;\ IT = 0|\hat{G}|0g_{9/2}0f;\ IT = 0>$ with $0f$ denoting either the $0f_{5/2}$ or the $0f_{7/2}$ orbit. The single particle energies had been adjusted in MONSTER(HFB) calculations [12] for «well deformed» odd mass nuclei in the $A \sim 50$ and $A \sim 80$ mass regions. The such defined Hamiltonian was then kept fixed and used for EXCITED VAMPIR and EXCITED FED VAMPIR calculations in several doubly even Ge, Se and Kr isotopes.

For the corresponding *complex* calculations 72 single particle states above the ^{40}Ca core (the same core as for the *real* calculations) were available for the about 30 valence nucleons. Here the $1p_{1/2}$, $1p_{3/2}$, $0f_{5/2}$, $0f_{7/2}$, $1d_{5/2}$, and $0g_{9/2}$ oscillator orbits for both protons and neutrons had been taken as model space. Consequently, a slightly modified monopole shift for the above-mentioned $T = 0$ matrix elements was used in the normalization of the G-matrix [23].

3. SHAPE COEXISTENCE IN THE $A \sim 70$ REGION WITHIN THE *REAL* EXCITED VAMPIR APPROACH

The basic idea of the EXCITED VAMPIR approach is to obtain optimized mean fields for each state of a given symmetry separately. In a chain of

variational calculations for projected determinants starting from the lowest state for a given angular momentum and parity I^{π} and then stepping up from one state to the next lowest one for the same I^{π}, with the current test wave function always being constrained to be orthogonal to all the solutions already obtained, one can describe states of very different structure. Therefore this approach should also allow one to describe the shape coexistence which is suggested by the data in the Ge and Se nuclei. One even could go so far and say that the complex situation encountered in the $A \sim 70$ region is a challenging testing ground for this theoretical model.

3.1. Low-Spin States in Even-Even Ge and Se Isotopes. The first insights into the complex structures of the nuclei in the $A \sim 70$ mass region came out from the investigation of the low-spin states in some chains of even Ge and Se nuclei in the frame of the *real* EXCITED VAMPIR model [13]. This approach yields indeed in all the considered doubly-even Ge and Se isotopes always some low-lying 0^+ and 2^+ states in the first few MeV excitation energy, as observed experimentally. In Fig.1 we show the energies of all the calculated and experimentally known 0^+ states in the ^{68,70,72,74}Ge isotopes. The maximum number of A-nucleon REV configurations for one angular momentum built by EXCITED VAMPIR variational procedure was five. One obtains VAMPIR wave functions, which are orthogonalized to each other, in various local minima. The $A \sim 70$ region is a good example to illustrate the power of this EXCITED VAMPIR method since one expects due to the various gaps in the Nilsson spectrum minima at rather different deformations. As a first state in a successively created optimal basis of A-nucleon configurations the most bound from the projected determinants so produced is taken. For the next states of the form (2.21) the variational principle guides us to choose the n-th projected determinant. Diagonalizing the residual interaction within the lowest m variational states one obtains the best possible description of the m lowest states of the considered spin value, which can be achieved by m projected HFB-type quasiparticle determinants. Of course, increasing the number of successive solutions m, we improve the structure of any wave function of the type (2.22) since the diagonalization of the residual interaction between more orthogonal states introduces more correlations in the final REV wave functions.

To get an idea about the structure of the *real* EXCITED VAMPIR wave functions for low-spin states in the investigated Ge and Se isotopes we display in Figs.2 and 3 some typical information. In these figures we show for all REV 0^+, 2^+, and 4^+ states in ^{70,72}Ge nuclei the intrinsic quadrupole moments for both neutrons (circles) and protons (squares) for the i-th projected determinant $|\phi_i^s>$ and for the 2^+ and 4^+ states the corresponding values

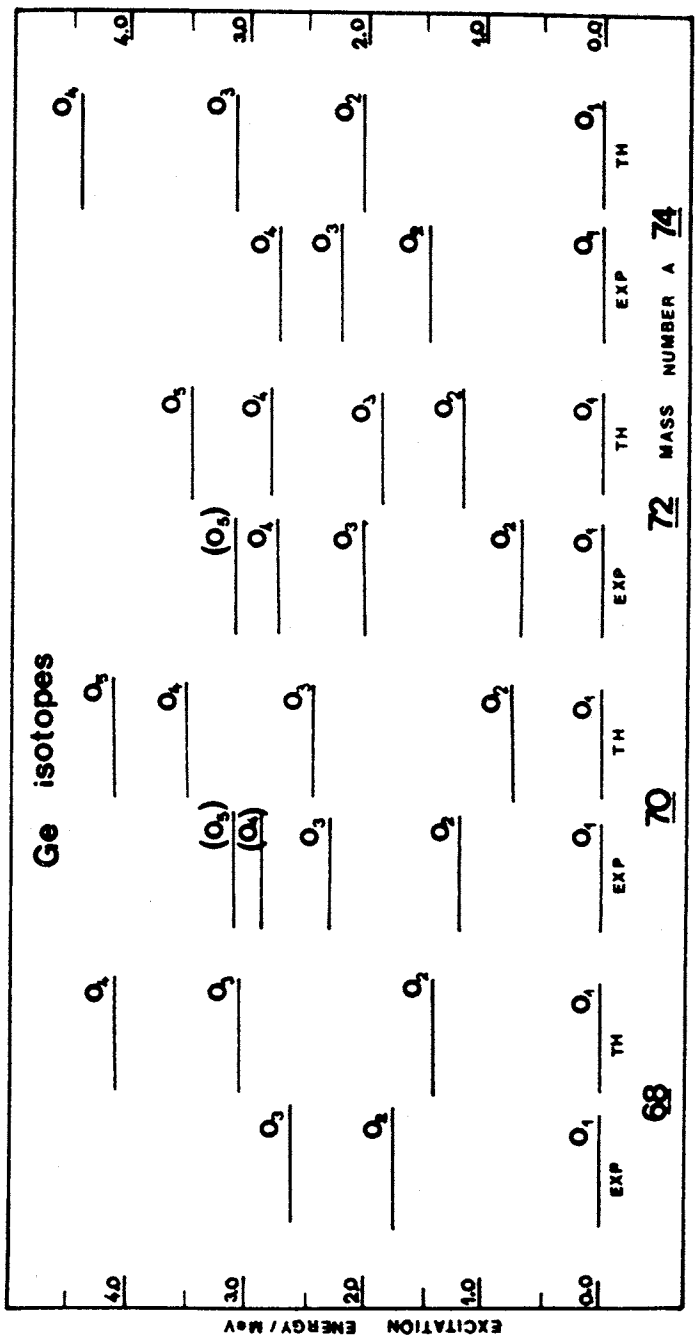

Fig.1. Comparison of theoretical and experimental energy trends for the 0^+ states in the investigated Ge isotopes

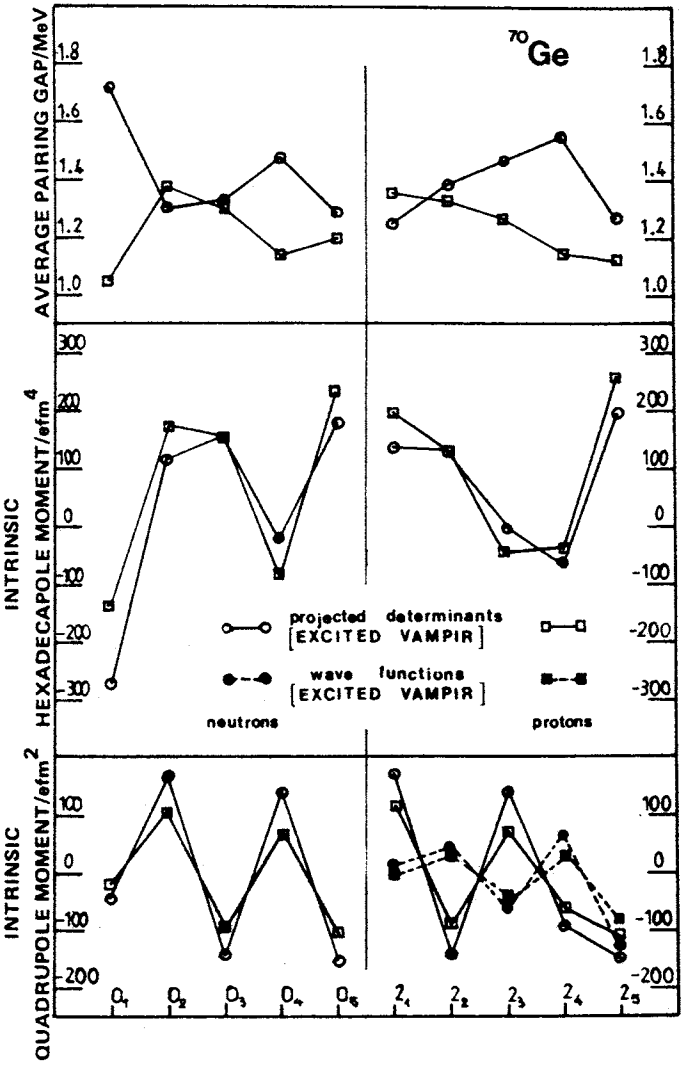

Fig.2. The intrinsic neutron and proton quadrupole and hexadecapole moments of the lowest five projected quasiparticle determinants obtained by the REV procedure for the 0^+ and 2^+ states in ^{70}Ge and the intrinsic quadrupole moments obtained from the corresponding spectroscopic value for the final REV wave functions, eq.(2.22) (full symbols are used). No effective charge has been used. The average neutron and proton pairing gap is given also for the above specified determinants. Squares refer to the proton, circles to the neutron, open symbols are for projected determinants

calculated from the spectroscopic quadrupole moments of the physical states. Due to the strong mixing of prolate and oblate projected determinants in the final wave functions the intrinsic quadrupole moments are often drastically reduced with respect to those of the projected nonorthogonal determinants. Moreover, even the sign of the intrinsic quadrupole moment for a state may appear changed with respect to that for the corresponding dominant determinant of the i-th variational solution as it is the case for the second, third and fourth 2^+ states in ^{70}Ge and second 2^+ state in ^{72}Ge. The nature of each projected determinant included in the calculations for a given symmetry s is pictured in Figs.2 and 3 by the intrinsic quadrupole and hexadecapole moments and the average pairing gaps. The mentioned quantities are given for both neutrons and protons. The average pairing gaps are defined here in

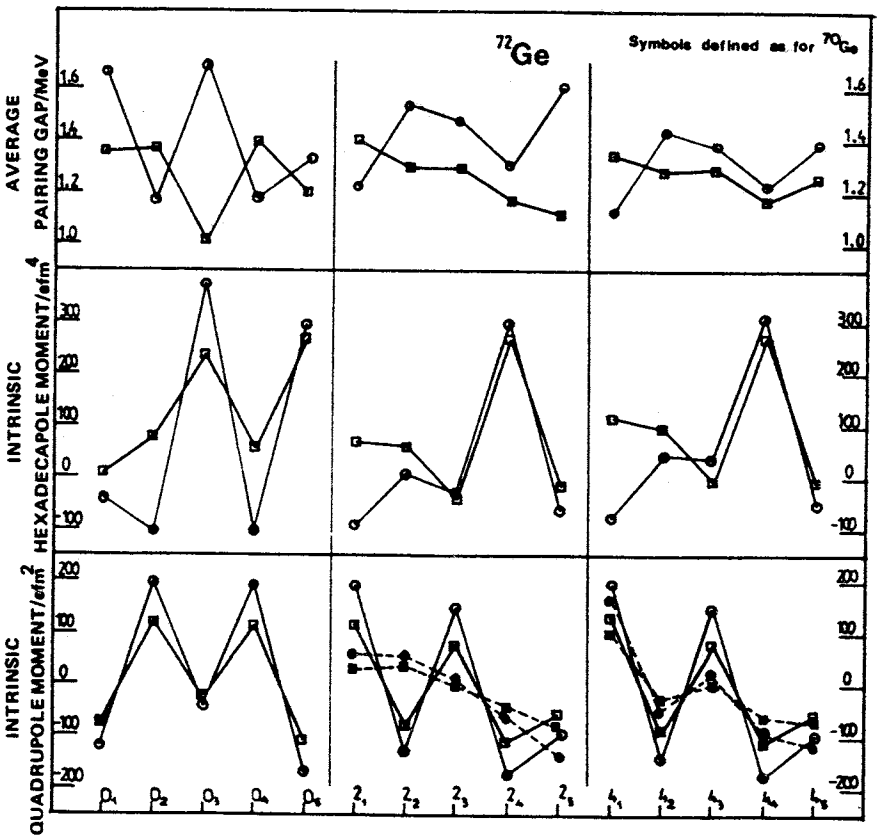

Fig.3. Same as in Fig.2, but for calculated 0^+, 2^+ and 4^+ states in ^{72}Ge

the usual way [25] as mean eigenvalues of the corresponding HFB pairing matrices $\Delta(\tau)$:

$$\Delta^{\tau}_{\text{aver}} \sim (1/M_{\tau}) \text{ tr } \Delta(\tau), \tag{3.1}$$

where

$$[\Delta(\tau)]_{ik} \sim \frac{1}{2} \sum_{r,s}^{(\tau)} v\,(ikrs)\,(B^{*}A^{T})_{rs} \tag{3.2}$$

is the (M_{τ} by M_{τ}) pairing matrix. A and B are the HFB transformation matrices of Eqs.(2.2) and (2.3).

The shape coexistence in the Ge isotopes is corroborated by our results. A tendency from an almost pure oblate small deformed 0^{+} ground state in ^{68}Ge to a strongly mixed prolate-oblate one in ^{72,74}Ge is predicted. For the ground states of the studied Se nuclei a tendency to an increasing prolate mixing going from 72 to 74 isotopes can be observed. For the excited 0^{+} states both Ge and Se isotopes manifest a strong prolate-oblate mixing.

More information about the structure of the ground and the first two excited 0^{+} states can be obtained from the spherical occupations of both neutron and proton orbitals illustrated in Figs.4 and 5. From the trend of the proton and neutron spherical occupation number we can learn more about the similarities and the differences concerning the structure of a particular state in a chain of isotopes and we can also easily compare these properties for a given symmetry s in a chain of isotopes. The theoretical results for the proton number occupations for the ground state in the Ge and Se considered isotopes are in good agreement with the experimental results obtained from (d, ^{3}He) transfer reactions on Ge and Se targets [26,27] and also from (p, t) reactions [28—30].

Besides the energies of the low excited low-spin states and neutron and proton spherical occupations for 0^{+} states in these calculations also the dependence of the deformation on the mass-number as manifested in the spectroscopic quadrupole moments of the 2^{+} yrast-states and the $E0$ transition probabilities in between the first excited 0^{+} states and the ground states could be well accounted for. The general trends in the quadrupole moments and $E0$ transition probabilities are in fair agreement with the available experimental data [31—33] as can be seen from Figs.6,7.

Indeed the EXCITED VAMPIR approach is able to describe the shape coexistence phenomena very nicely. The results indicate that for low angular momenta configurations with different deformations are not only «coexisting» but do mix strongly with each other. The REV wave functions for the low-spin states in this mass region are in general complicated mixtures of several configurations corresponding to rather different deformations, with a special interplay of the prolate and oblate deformed mean fields and dynamical

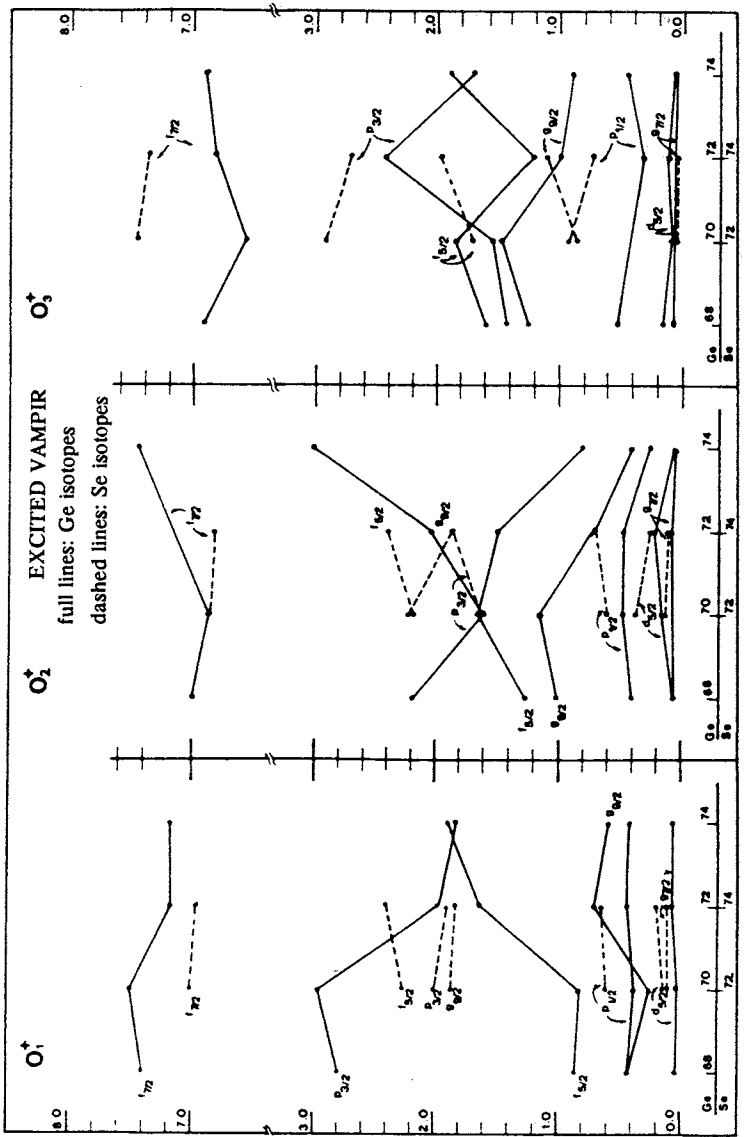

Fig. 4. Significant proton occupation numbers of the spherical-basis orbitals for the lowest three 0^+ states in the investigated Ge and Se isotopes. Full lines are for Ge nuclei; dashed lines, for Se nuclei

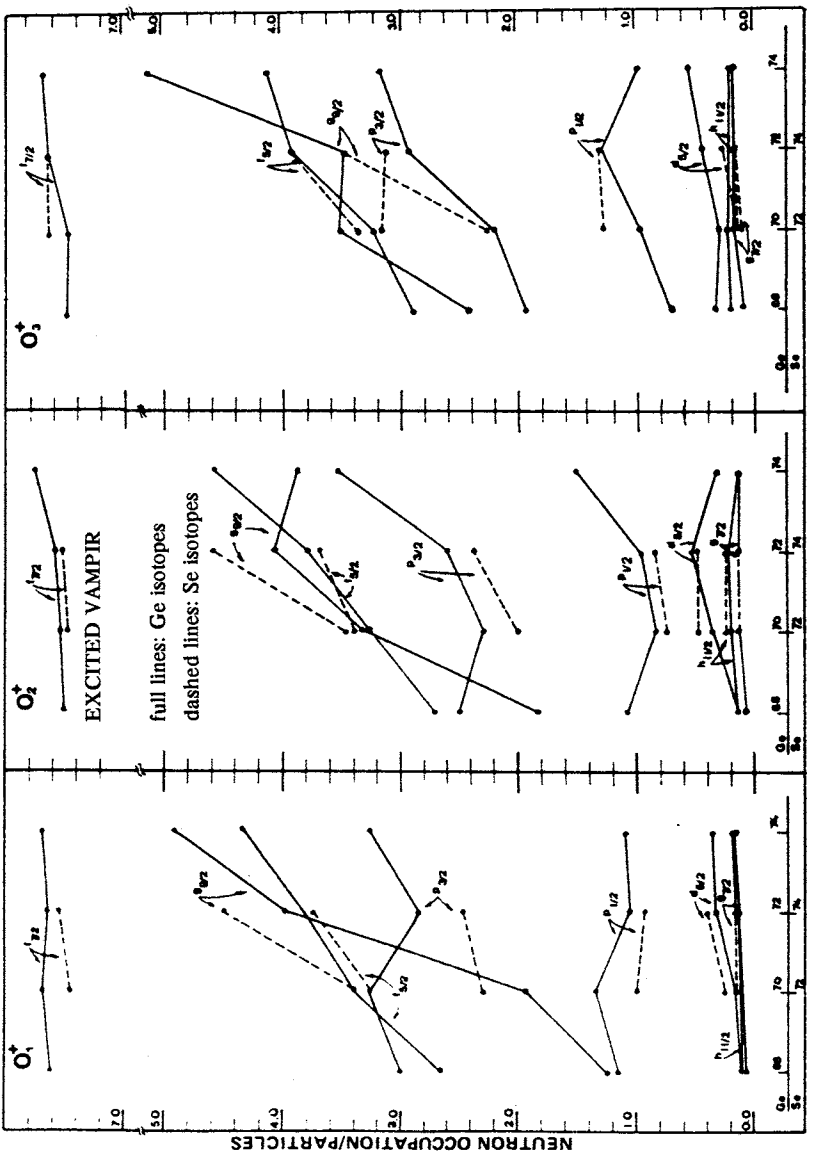

Fig.5. Same as in Fig.4, but for the neutron occupations

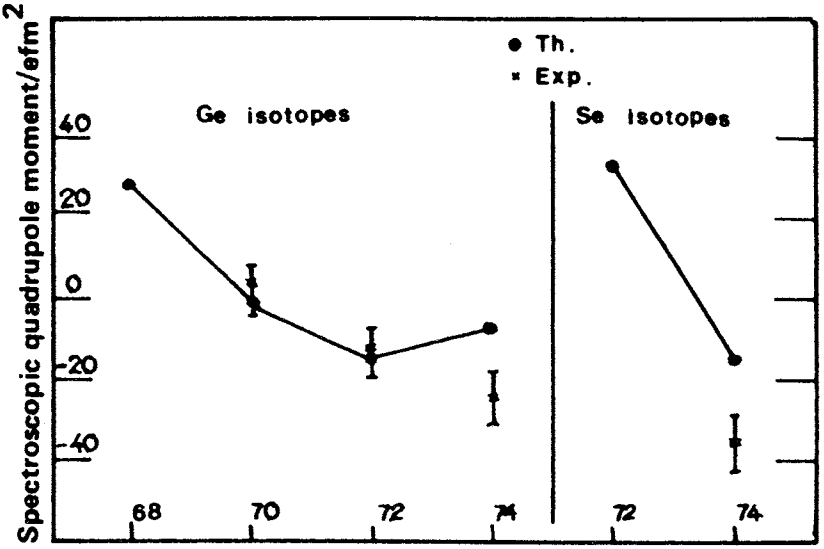

Fig.6. Comparison of the theoretical spectroscopic quadrupole moments for the first 2^+ states in the investigated Ge and Se nuclei and the corresponding available data. The effective charge is $e_n = 0.25$ and $e_p = 1.25$

changes of the hexadecapole deformations. This holds especially for the 0^+ states, however, though with decreasing importance, considerable mixing is obtained also in the 2^+ and 4^+ states.

3.2. High Spins in ^{68}Ge, ^{70}Se and ^{72}Se Nuclei. These encouraging results and the experimental evidence concerning the triple forking at 8^+ into three bands with no crossing transitions observed earlier [34] gave us motivation to extend our studies to states with higher angular momenta to investigate whether the shape coexistence does persist also at high spins. In the frame of the *real* EXCITED VAMPIR approximation we extended our investigations to spins up to 18^+ in ^{68}Ge and ^{70}Se and up to 22^+ in ^{72}Se. Note, that these calculations have been accomplished using the same model space and effective Hamiltonian as for the low spin states.

For the description of the structure of the high-spin states up to $m = 8$ A-nucleon EXCITED VAMPIR configurations of the type (2.21) for each considered angular momentum were taken into account. It turned out that the *shape coexistence*, i.e., the occurrence of various states with the same spin being based on configurations with different deformations within a small interval of excitation energy, indeed persists even at rather high-spin values.

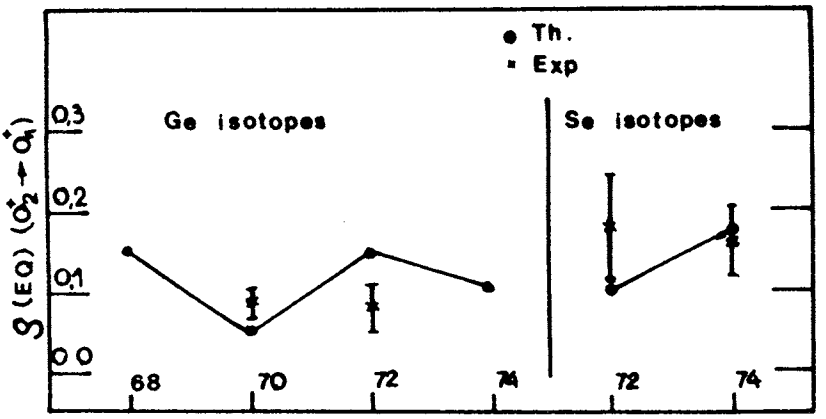

Fig.7. Comparison of the theoretical $E0$ transitions $\rho(E0; 0_2^+ \rightarrow 0_1^+)$ in the investigated Ge and Se nuclei and the corresponding available data. Effective charges $e_n = 0.25$ and $e_p = 1.25$ have been used

As it is expected from the different gaps characterizing the Nilsson scheme for the nuclei in the $A \sim 70$ mass region we obtained for each considered spin many different HFB-type projected determinants corresponding to very close-lying local minima. These determinants can differ, e.g., in the sign and/or magnitude of the intrinsic quadrupole moments, or in some cases, e.g., only in the sign and/or magnitude of the intrinsic hexadecapole moments which play a very special role in all three nuclei ^{68}Ge, ^{70}Se, and ^{72}Se, favouring in some cases the alignment of the neutrons occupying the spherical $g_{9/2}$ state.

The orthogonal variational states (2.21) produced by REV procedure and finally the physical states (2.22) obtained by the diagonalization of the residual interaction are still very close in energy. In all three nuclei we have obtained 4—5 states of a given spin (8^+, 10^+, 12^+, 14^+) bunched whithin only 1.5 MeV. The theoretical results presented in Fig.8 for ^{68}Ge and in Figs.9 and 10 for ^{70}Se and ^{72}Se, respectively, reveal a special feature: most of the high spin states are decaying in many various ways. Note, that the experimental spectrum given in Fig.8 for ^{68}Ge was the only one available at the time when we accomplished our REV calculations. Recent experimental data [17] give support to our predictions. These will be presented later and compared with the results of more sophisticated investigations using the *real* EXCITED FED VAMPIR approach.

We analysed all the possible decay paths starting from the states with the highest calculated spin in each nucleus. Since we have so many states for each

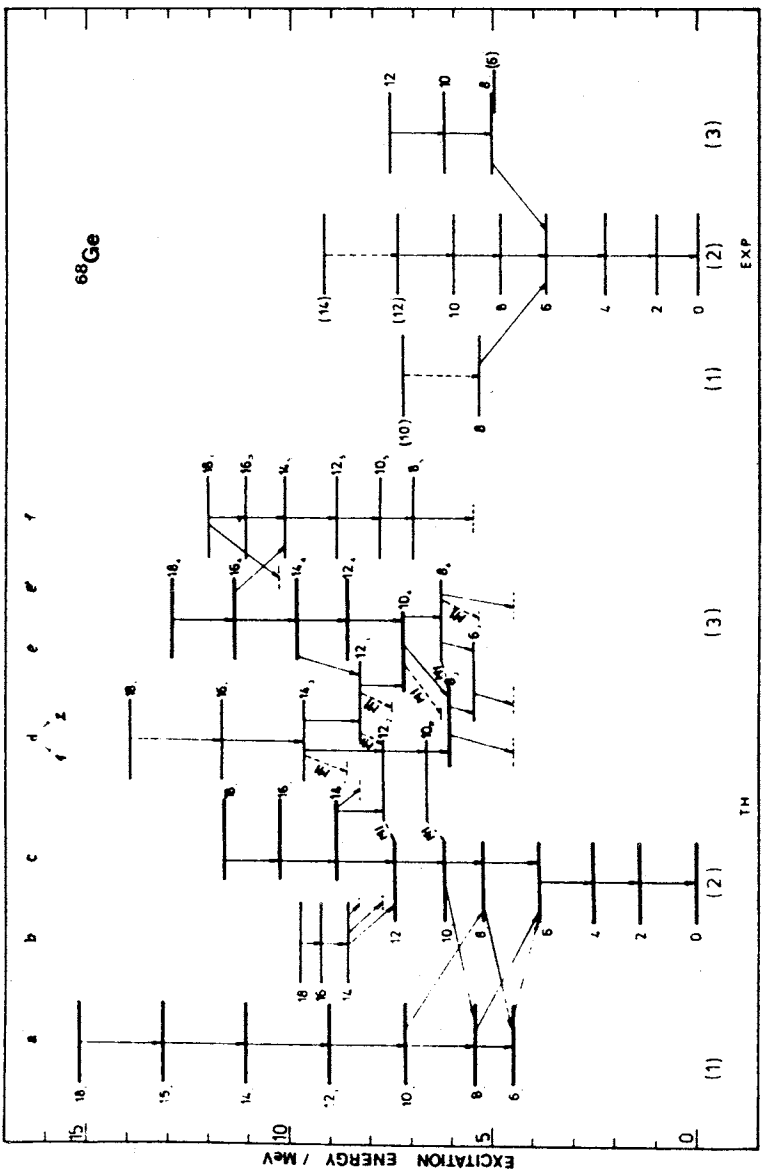

Fig.8. The theoretical spectrum of the nucleus ^{68}Ge here obtained in the *real* EXCITED VAMPIR approximation is compared with the experimental data from de Lima et al. [34]

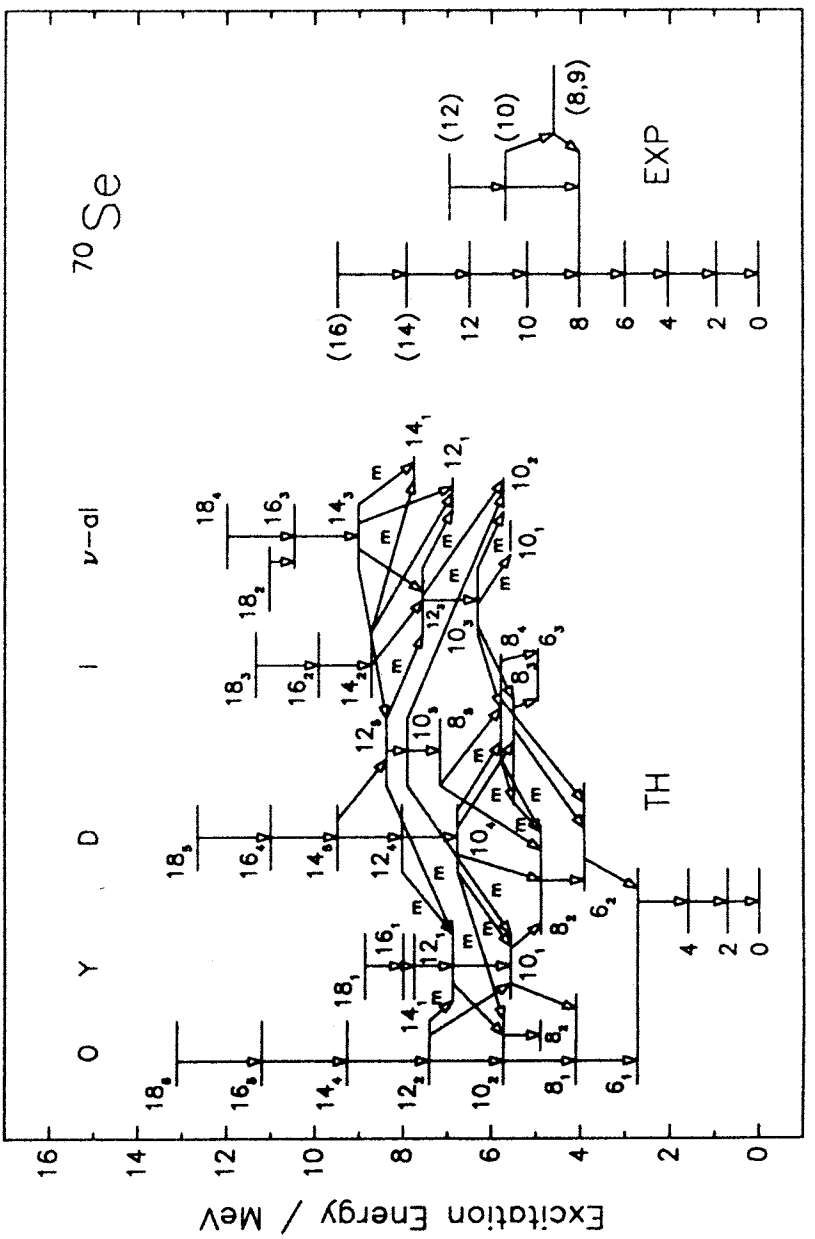

Fig.9. The theoretical obtained spectrum for ^{70}Se within the *real* EXCITED VAMPIR approach is compared with the available experimental data [35,36]. The labels indicating the classification of the various theoretical bands are explained in the text, and the «*m*» at some of the decay-links refer to strong $\Delta I = 0, M1$ transitions

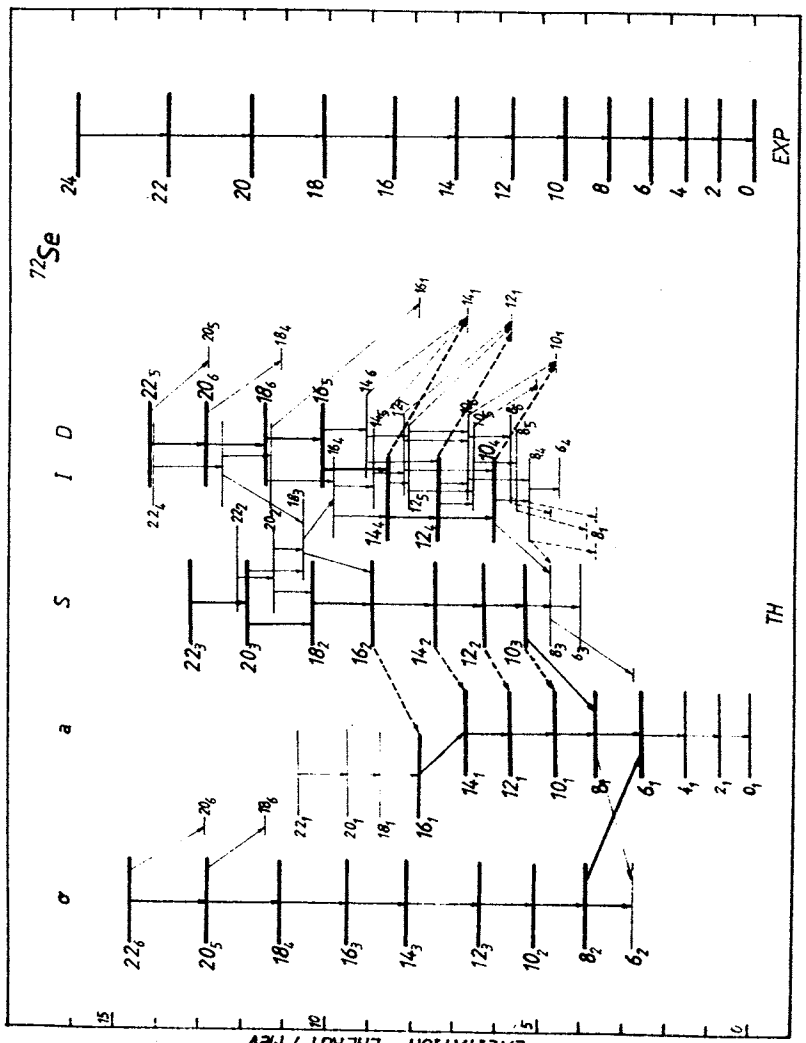

Fig.10. The theoretical spectrum for ^{72}Se obtained in the real EXCITED VAMPIR approximation is compared with the experimental data [17,36]. The labels of the theoretical bands are explained in the text and the dashed lines indicate strong $M1$, $\Delta I = 0$ transitions

spin bunched so much in energy, decaying by many branches, and as the measured $B(E2)$ values reported by different experimental groups are very spread and involve large error bars which arise due to the uncertainties associated with the feeding times, we can always suggest a few «most probable» paths of the cascades leading to the yrast 6^+ state which are compatible with the presently available experimental data. The situation becomes even more complicated since we found strong $M1$, $\Delta I = 0$ transitions which in some cases are much faster than the intraband $E2$ transitions. We classified the calculated levels into different collective bands solely on the basis of the $B(E2)$ values amongst them. Then for all three nuclei we tried to find the fastest ways to enter the yrast line and so to identify the most probable candidates for the experimental linkages of the measured gamma rays in bands.

In all three nuclei an oblate band (the most left one in the theoretical spectrum always) coexists with many other prolate bands. For the higher spins the oblate bands consist of the highest calculated states of a given angular momentum. In the theoretical spectra the label for each spin corresponds to the energetical order in the calculated set of states for a given angular momentum.

In ^{68}Ge the yrast band is mainly oblate up to spin 6^+. The strongest oblate-prolate coexistence is obtained for the first two 8^+ states. Starting with spin 10^+ a pure oblate band is emerging which coexists with all the other prolate bands. No feeding from this oblate band to the prolate bands exists above spin 10^+. With respect to the other calculated bands, however, these oblate states are at rather high excitation energy and therefore probably only weakly populated. Concerning the other bands presented in Fig.8 these are pure prolate bands for spins $I \geq 10$. The structure of the wave functions for the $I^\pi = 10^+, 12^+, 14^+$ states shows a rather strong mixing of various mean fields differing by the neutron and proton intrinsic quadrupole and hexadecapole deformations. This shape coexistence explains the appearance of two or three comparable fast transitions decaying a given state, as can be seen in Fig.8, which was later confirmed by experiment (Fig.23). The various mean fields dominating the structure of the wave functions for the other spins also have different neutron and proton intrinsic quadrupole and hexadecapole moments. Protons and neutrons equally contribute to the special structure of the high-spin bands. In Fig.11 we display the proton and neutron intrinsic quadrupole moments for the three fastest decaying prolate bands and for the oblate band. The labels of the bands are the same as in Fig.8.

A measure of the deformation characterizing the different bands is offered by the theoretical and experimental evaluated $B(E2, \Delta I = 2)$ values [34,37—39] given in Table 1. The agreement of the theoretical $B(E2)$ values

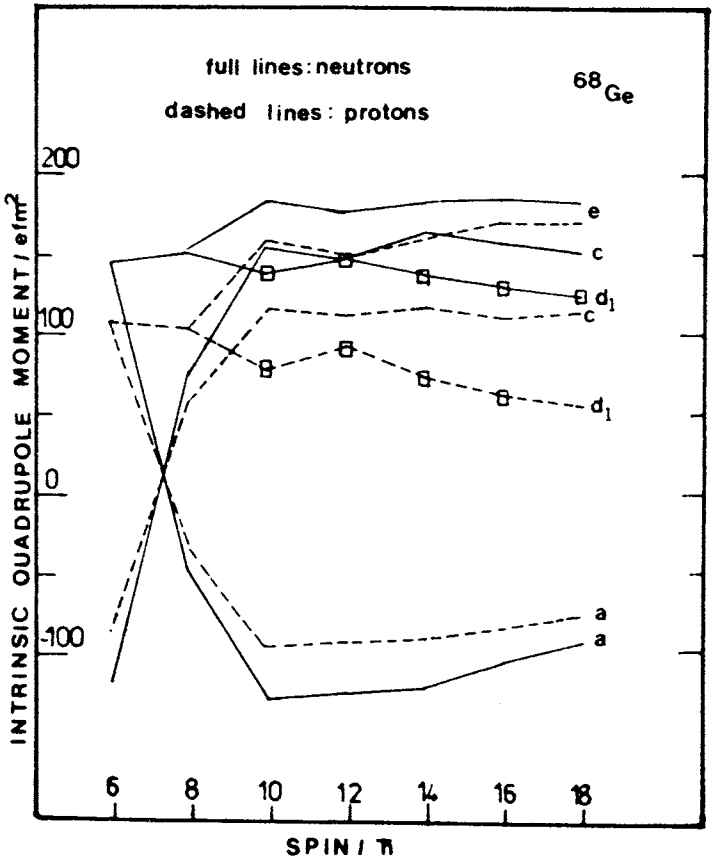

Fig.11. The intrinsic neutron and proton quadrupole moments obtained from the corresponding spetroscopic values for the states belonging to the specified (a, c, d_1,e) bands in ^{68}Ge in the REV approximation. No effective charge has been used. Full lines are for neutrons; dashed lines, for protons

with the experimental data is rather poor, even if one takes into account the large error bars and the large spread in these data obtained by different groups. As the side feeding in this mass region is still an open problem [4], we did not intend to fit these data. Therefore for all the investigated nuclei the same values of the effective changes and the same renormalization of the effective Hamiltonian were used.

In Fig.12 we give the neutron and proton intrinsic hexadecapole moments of the bands calculated in ^{68}Ge in the REV approximation. A special trend is displayed by the d_1 band which is in fact a neutron-aligned band: for the 8_3^+

Table 1. Some calculated (REV) and experimental [34,37—39] $B(E2, I_i \to I_f)$ (e^2fm^4) values for the nucleus ^{68}Ge. The effective charges were $e_n = 0.25$ and $e_p = 1.25$

I_i	I_f	Theory	Experiment		
			a)	b)	c)
2	0	181	251^{+126}_{-63}	150^{+100}_{-56}	129±30
4	2	633	177^{+64}_{-37}	221^{+70}_{-60}	204±110
6	4	834	197^{+78}_{-44}	196±50	> 137
8_y	6_y	503	281^{+70}_{-47}	600^{+100}_{-130}	220±60
8_r	6_y	3	260±100		
8_l	6_y	395	50±20	79±30	
10_y	8_y	811	410±110	457^{+114}_{-130}	760^{+380}_{-300}

y — yrast, l — left and r — right bands in Fig.8.
a) ref. [34,37], b) ref. [38], c) ref. [39].

state the hexadecapole moments are much smaller than for the 8_1^+ and 8_2^+ states and the neutron Q_4 moment is negative. Except for the 12_2^+ state which still has the smallest hexadecapole moments from all displayed 12^+ states the neutron and proton Q_4 moments are negative for all the higher spin states of the d_1 band. A qualitative understanding of the effect of hexadecapole deformation on the orbitals lying around the Fermi level can be obtained in the framework of a simple perturbation treatment applied on a Nilsson-type axially deformed potential including an Y_{40} deformation [41]. The wave functions for the 10^+, 14^+, 16^+, 18^+ spin states belonging to the d_1 band are based essentially on a single VAMPIR determinant, prolate deformed, with the smallest found quadrupole deformation for both neutrons and protons, slowly decreasing with increasing spin. The 8_3^+ and 12_2^+ states of the d_1 band are mixed states based on coexisting mean fields with positive and negative hexadecapole moments. The contribution of the $g_{9/2}$ neutrons to the intrinsic hexadecapole moment is very small in the d_1 band and becomes even negative for some spins. For the case of a negative hexadecapole moment the simple perturbation treatment predicts that the $m = 1/2$ $g_{9/2}$ orbital moves to the Fermi level favouring the alignment of the two neutrons occupying the

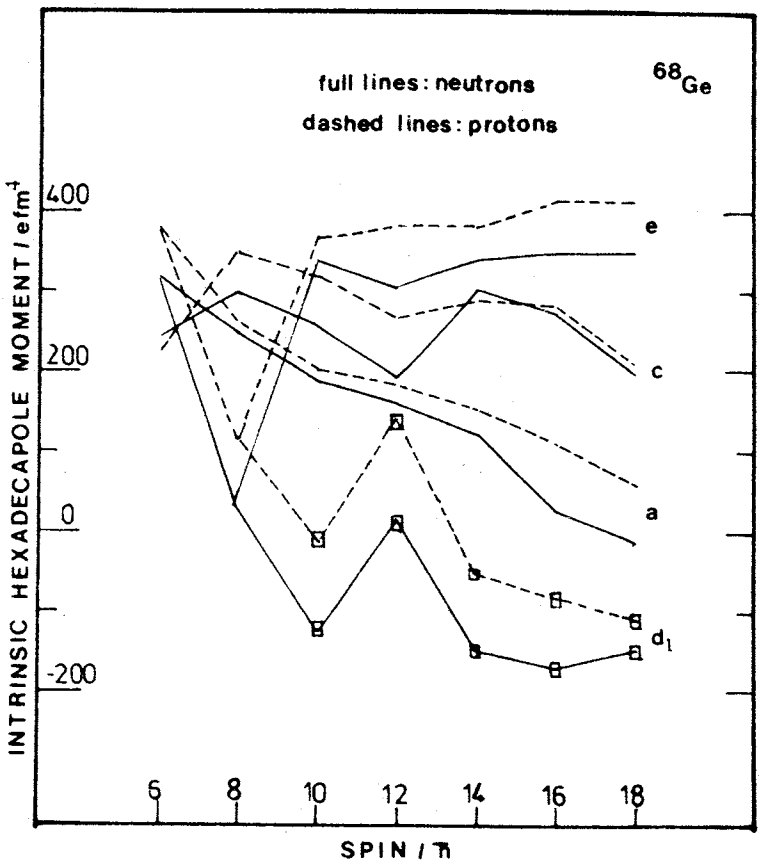

Fig.12. The intrinsic neutron and proton hexadecapole moments obtained from the corresponding calculated values in the laboratory system for the states belonging to the specified (a, c, d_1,e) bands in ^{68}Ge in the REV approximation. No effective charge has been used. Full lines are for neutrons; dashed lines, for protons

spherical $g_{9/2}$ state. This effect can also be seen in our wave functions. The proton occupation of the $g_{9/2}$ orbital is slowly going down to zero with increasing spin for d_1 band states, and consequently a sharp alignment of the neutrons is very much favoured. This strong neutron alignment is reflected in the small g-factors of the states belonging to the d_1 band which become even negative for the spin 8^+ and 10^+ states. Therefore, the 8_3^+ state rather likely

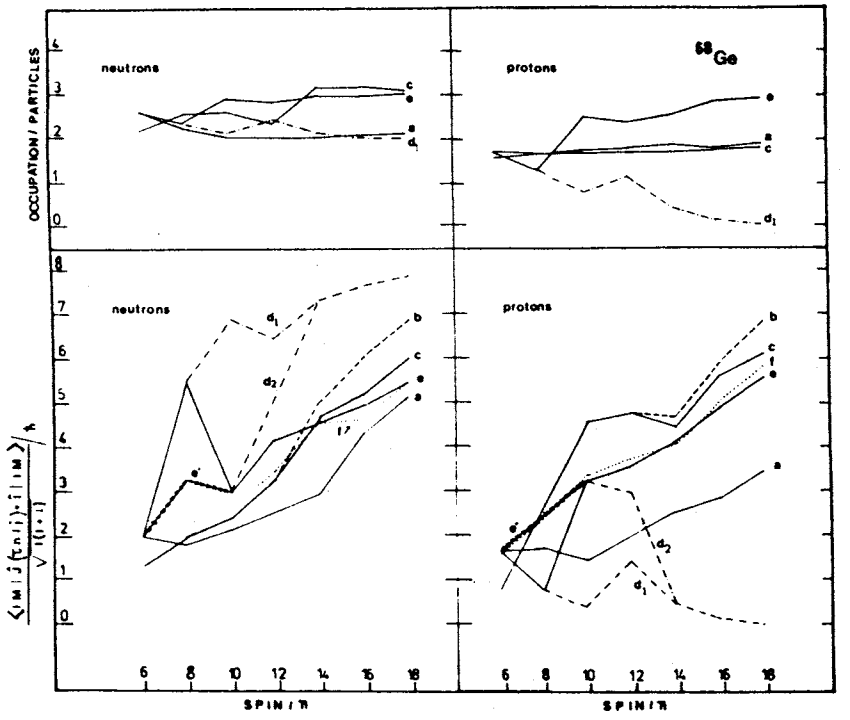

Fig.13. The alignment plot (bottom part) representing the normalized angular momentum contribution of the neutrons (left) and protons (right) filling the $g_{9/2}$ spherical basis state in the direction of the total angular momentum I for the positive parity states of the REV bands calculated in ^{68}Ge. In the upper part of the figure the neutron (left) and the proton (right) occupation numbers of the spherical $g_{9/2}$ for some of the theoretically obtained bands in ^{68}Ge are given

corresponds to the experimental 8_2^+ for which a g-factor of -0.28 ± 0.14 has been measured [42].

A picture revealing a possible sharp alignment of the angular momenta of the particles occupying the high-j spherical orbital ($g_{9/2}$ for the $A \sim 70$ region) with respect to the total angular momentum is given in Fig.13. The normalized angular momentum contribution of the $g_{9/2}$ neutrons and protons in the direction of the total angular momentum I is given by

$$\mathbf{J}(\tau nlj) = \frac{\langle \Psi; sM | \hat{\mathbf{J}}(\tau nlj) \cdot \hat{\mathbf{I}} | \Psi; sM \rangle}{\sqrt{I(I+1)}}. \tag{3.3}$$

In Fig.13 we present the resulting alignment plots (bottom part) and the occupation numbers (upper part) for the neutrons (left) and protons (right) filling the $g_{9/2}$ spherical single-particle state. A sharp alignment of the neutrons is evident going from 6_2^+ to the 8_3^+ state. This strong alignment dominates the d_1 band. Except for the 12^+ state the neutron occupation number is very close to two particles for all the states belonging to this band. At the same time the protons from the $g_{9/2}$ orbital almost do not contribute to the total angular momentum of the states. This can be understood from the continuous depletion of this orbital with increasing spin. This is a normal trend created by the gradual decrease of the intrinsic quadrupole moment, well distinguished in Fig.11. A sharp proton alignment characterizes the yrast band (*c*) going from spin 6 to 10. For higher spins in this band protons and neutrons make a comparable moderate contribution to the total angular momentum. The alignment of the particles in the $g_{9/2}$ orbital is reflected by the *g*-factors plotted in Fig.14.

Our calculations revealed some strong $B(M1, \Delta I = 0)$ transitions for ^{68}Ge indicated in Fig.8 by dashed lines. Predicted by Frauendorf in the framework of the cranked shell model [43] and measured by Funke et al. [44] in even and odd Kr isotopes such strong $\Delta I = 0$, $M1$ transitions between states of crossing bands should be expected. All these strong $M1$ transitions are dominated by $g_{9/2}$—$g_{9/2}$ recoupling terms, i.e., they result mainly from a reordering of the particles in this orbit in the final with respect to the initial state. Spin- and orbital-contributions to the transition amplitudes are of about the same size with, in general, a slight dominance of the latter. So, e.g., in the largest $M1$ ($B(M1) = 2.56\mu_N^2$), connecting two 8^+ states, the total transition amplitude is $-6.60\mu_N$. From this value comes $-2.23\mu_N$ from the neutron-spin and $-0.84\mu_N$ from the proton-spin parts. The proton orbital contribution on the other hand is $-3.63\mu_N$. The latter value can be decomposed into $-2.04\mu_N$ from the diagonal $g_{9/2}$-, $-0.82\mu_N$ from the diagonal $f_{7/2}$- and $-0.52\mu_N$ from the diagonal $f_{5/2}$-single-particle transition matrix elements (the rest is distributed over many different spectroscopic amplitudes). These strong $M1$ transitions are an interesting result of the calculations. These predictions concerning the fast $M1$ transitions complete the picture of the most probable parths of feeding the investigated states.

We shall now consider the nucleus ^{70}Se which has two more protons with respect to the nucleus ^{68}Ge. The investigations of the features of ^{70}Se have been performed in the frame of the *real* EXCITED VAMPIR approximation, using the same model space and effective Hamiltonian as above. Here have

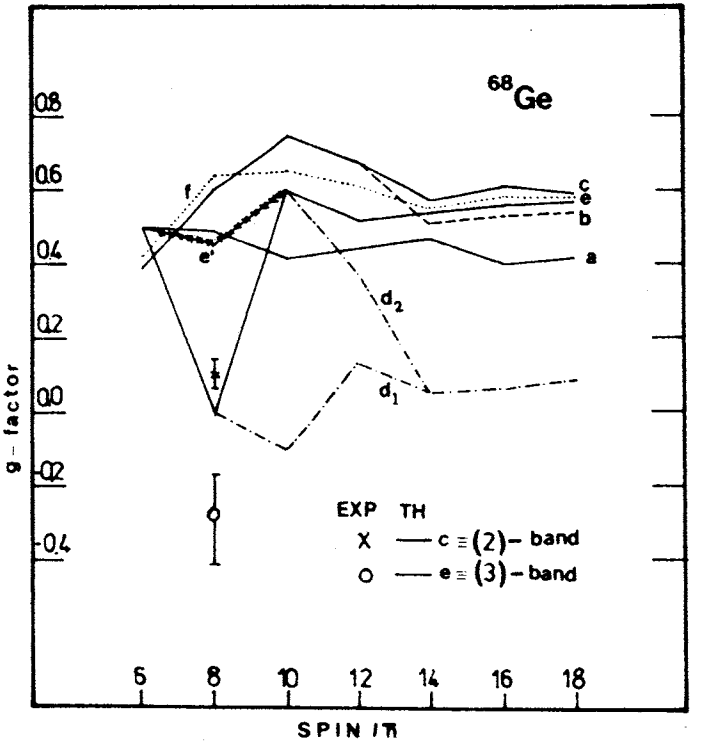

Fig.14. The g-factors of the REV bands in ^{68}Ge and the available data for some 8^+ states. The calculated bands labelled c and e are associated to the experimental bands classified as (2) and (3), respectively. Free values for the neutron and proton g-factors have been used in the calculations

been calculated the lowest six 0^+, 2^+, 8^+, 10^+, 12^+, 14^+, 16^+ and 18^+ as well as the lowest five 4^+ and 6^+ states and after the diagonalization of the residual interaction the solutions have been grouped again into various bands entirely on the basis of the $B(E2)$ values. A rather complicated decay pattern with a high level density in certain spin region can be seen in the spectrum given in Fig.9. The structure of the various bands can be summarized as follows:

Up to angular momentum 8^+ the yrast states are almost pure oblate configurations. This oblate band O then continues with the second 10^+ state which, however, has a strongly mixed wave function with a large prolate component. Above the second 12^+ which still displays some oblate-prolate mixing the band then continues with the fourth 14^+, the sixth 16^+ and again

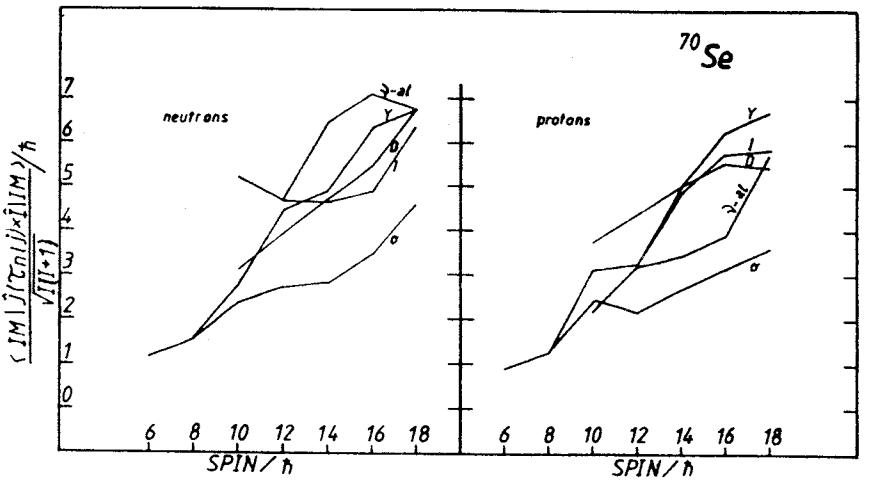

Fig.15. The neutron and proton alignments of the $0g_{9/2}$ orbit as in the bottom part of Fig.13, however, for the nucleus ^{70}Se studied in the REV approximation

the sixth 18^+ solutions which again have rather pure oblate deformed configurations. As in ^{68}Ge the protons and neutrons in the $0g_{9/2}$ shell-model orbit do both contribute only little to the total angular momentum of this oblate band as can be seen from Fig.15 where the corresponding alignments are plotted.

The other four bands displayed in Fig.9 are again all prolate deformed as can be seen from the spectroscopic quadrupole moments in Table 2. Most of them have furthermore similar structure as the bands of ^{68}Ge discussed above. The band labelled as *D* is strongly deformed (the dominant determinant in the 14^+_5 state having a quadrupole deformation of $\beta_2 \sim 0.32$). The neutron-aligned band $\nu - al$ is a moderately deformed band and the $0g_{9/2}$ neutrons are responsible for a considerable portion of the total angular momentum. As a consequence the *g*-factors in this band are distinctly smaller than in all of the other bands being presented. As compared to the case of ^{68}Ge, however, the neutron alignment in the ^{70}Se band is less pronounced. This is due to the fact that in the ^{68}Ge band there are just two $0g_{9/2}$ neutrons while the proton $0g_{9/2}$ orbit is almost empty. Thus the neutron alignment is very much favoured. In ^{70}Se, however, we have two additional protons which partly occupy the $0g_{9/2}$ and also lead to a somewhat larger neutron occupation of this level. Thus here the alignment does not happen as rapidly as in the

Table 2. The spectroscopic quadrupole moments Q_2^{sp} $(e\cdot\mathrm{fm}^2)$ for some of the REV bands obtained for the nucleus ^{70}Se and displayed in Fig.9. As effective charges again the same values as in ^{68}Ge have been taken. The labels $(O, Y, D, I, \nu{-}al)$ referring to the various bands are explained in the text

$I[\hbar]$	O	Y	D	I		$\nu{-}al$
2	43					
4	61					
6	68					
8	69					
10	20	−26	−101		−78	
12	56	−75	−98		−70	
14	66	−77	−100	−81		−83
16	63	−79	−99	−80		−78
18	59	−79	−84	−81		−84

former case. Adding two more neutrons the occupation of the $0g_{9/2}$ orbit is increased even more, the alignment severely hindered, and this is the reason why no equivalent band was found in the case of ^{72}Se, which will be discussed below. As a consequence of the less pronounced alignment the neutron-aligned band in ^{70}Se starts with a g-factor of still 0.24 for the 10_3^+ solution while in ^{68}Ge the g-factor of the 8_3^+ band head was even reduced to −0.03. Parallel to the neutron-aligned band another moderately deformed prolate band labelled I in Figs.9 and 15 and in Table 2 is obtained. Below angular momentum 14 these two bands having rather similar spectroscopic quadrupole moments and $B(E2)$ values become strongly mixed and follow essentially the same decay path. Both the 14_2^+ as well as the 14_3^+ feed via $M1$ transitions the yrast 14_1^+ and via $B(E2)$ transitions subsequently the 12_3^+ and 10_3^+ levels. These in turn decay via strong $M1$ transitions of $B(M1; 12_3^+ \to 12_1^+) = 2.01\mu_N^2$ and $B(M1; 10_3^+ \to 10_1^+) = 2.21\mu_N^2$ into the yrast level and because of the strong mixing of the lowest two 10^+ states a considerable $B(M1; 10_3^+ \to 10_2^+) = 1.32\mu_N^2$ leads into the oblate band, too. The two lowest 10^+ states then both decay preferentially into the oblate 8_1^+

configuration. The last of the above-mentioned four bands consists out of the yrast levels above spin 12^+. The band labelled as *Y* displays $B(E2)$ values being comparable to those obtained for the *O*-, the $\nu - al$- and the *I*-band. However, because of a rather small energy splitting within this band, especially in between its 16_1^+ and 14_1^+ members the corresponding decay path is relatively slow. We should mention here that the strongly deformed high-spin band found in the ^{68}Ge nucleus has no counterpart in the ^{70}Se nucleus at least in the present *real* EXCITED VAMPIR description. Obviously it cannot be excluded that such a band may be found at higher excitation energy in this nucleus, too.

It is worth mentioning that strong magnetic dipole transitions linking the various bands with each other in the intermediate spin region are obtained in ^{70}Se nucleus, too. As it was expected in this spin region a competition of several configurations resulting from the various possible couplings of the $0g_{9/2}$ valence protons and neutrons is revealed by the structure of the wave functions and in most cases the strong $B(M1)$ values are dominated by amplitudes corresponding to the reordering of nucleons in this shell-model orbit. As a consequence these transitions usually contain considerable (about 50%) orbital components.

Finally, few words concerning the comparison with the experimental data [35,36] which are presented in the right part of Fig.9. Up to angular momentum 8^+ we obviously have to identify the theoretical yrast states with the experimental ones. In this spin region the transition energies are in fair agreement and the $B(E2; 2_1^+ \rightarrow 0_1^+)$, too. On the other hand the experimental $B(E2)$ values for the $6_1^+ \rightarrow 4_1^+$ and the $4_1^+ \rightarrow 2_1^+$ are considerably smaller than those predicted theoretically. Here the inclusion of additional correlations within the EXCITED FED VAMPIR approach may help as well as a renormalization of the effective Hamiltonian which seems to be necessary as will be discussed later on in the context of these calculations. However, it cannot be excluded that the uncertainties in the feeding times [4] may lead to changes of the experimental data, too. Here, obviously, more information is needed before definite conclusions can be drawn. The same holds for the classification of the experimental levels above angular momentum 8^+. Here the present calculations offer three candidates: the oblate band, displaying the fastest decay, however, having a somewhat too small moment of intertia in this spin region, the deformed band *D* or the neutron-aligned band. These last two structures reproduce the experimental transition energies quite nicely, however, both imply an up to now unobserved strong magnetic dipole transition. Thus the present investigation can only be considered as a first guideline to the nucleus ^{70}Se and a lot more of both theoretical as well as

experimental studies seems to be required before a satisfactory understanding will be reached.

In order to obtain some more information about the systematic trends and variations in this mass region we investigated the low- and high-spin states of the nucleus ^{72}Se with two extra neutrons with respect to ^{70}Se and two neutrons and two protons more than ^{68}Ge. Again the same model space and effective Hamiltonian as for ^{68}Ge and ^{70}Se was used within the *real* EXCITED VAMPIR approximation.

In ^{72}Se the experimentally observed gamma rays are linked in a single positive-parity band up to spin 28^+ [17,36]. All crossing transitions to other side bands observed up to now have experimental branching intensities less than 10% of the observed cascade feedings. In ^{72}Se nucleus we analysed all the possible decay paths starting from the first six 22^+ states. Of course only positive parity even spin states have been investigated. Again the prolate-oblate coexistence dominates the structure of the low- and high-spin states in ^{72}Se. For the low-spin yrast states a dominant oblate character emerges from the structure of the wave functions and the spectroscopic quadrupole moments for 2_1^+ and 4_1^+ states. The strongest prolate-oblate mixing does appear for the 6_1^+ and 6_2^+ states. This strong mixing makes a small quadrupole moment for the 6_1^+ state. The first predominant oblate state of the band labelled (*o*) in Fig.10 is the 8_2^+ and so are all the higher spin states belonging to this band. The intrinsic quadrupole deformation of the oblate mean fields underlying the structure of these oblate band states varies very slowly and smoothly to smaller Q_2 values with increasing spin. The oblate band could be characterized as a vibrational band, with almost equidistant levels and nearly constant spectroscopic quadrupole moments. These $Q_2^s(I)$ are small compared to those of all the other analysed bands and the $B(E2)$ values are almost constant around 50 W.u. All the other bands presented in Fig.10 are prolate deformed bands as it is illustrated by the spectroscopic quadrupole moments for these states given in Table 3. Again effective charges of 0.25 for the neutrons and 1.25 for the protons were used. The large range of REV $B(E2)$ values (Table 3) characterizing the intraband $E2$ transitions reflects the various different quadrupole deformations.

Classifying the states in bands solely on the basis of the $B(E2)$ values we tried to find the fastest ways to enter the yrast line. The fastest prolate decaying paths are pointed out in Fig.10. However, a detailed look at the calculations reveals that there is a path of very fast cascade $E2$ transitions which cross from one band to another with the largest (*S-strong*) quadrupole deformation with only slow (weak) transitions to other states. Thus, it is

Table 3. REV spectroscopic quadrupole moments and $B(E2; I \to I-2)$ values for the states belonging to the specified (o, a, S, I, D) bands of the nucleus ^{72}Se. The available experimental results are given for comparison (refs.[40,45,46]). The labels of the bands are the same as in Fig.10. The effective charges were: $e_n = 0.25$ and $e_p = 1.25$

$I[\hbar]$	$Q_2^{sp}[e\cdot\mathrm{fm}^2]$							
	o	a	S	I	D			
2	34							
4	47							
6	−37	18						
8	67	−87	−96		−95			
10	76	−91	−99		−93			
12	73	−86	−107		−104			
14	76	−83	−111		−105			
16	76	−83	−113		−95 −97			
18	73	−83	−106	−81	−103			
20	49	−83	−110	−83	−81			
22	66	−83	−107	−85	−96			
$I[\hbar]$	$B(E2; I \to I-2)$ $[e^2\mathrm{fm}^4]$							
	Theory					ref.[45]	ref.[46	ref.[40]
2		627				400±50	356±36	427±53
4		996				1060±160	801±107	1085±160
6		1100				900±90	1068±178	907±71
8	734	869				1250±150	1263±142	1263^{+178}_{-142}
10	1067	1407				1510±180	1744±231	1512^{+231}_{-178}
12	1118	910	1371		1191		1637±178	1619^{+409}_{-267}
14	1044	920	1987		1606		2544^{+2544}_{-854}	2491^{+1495}_{-676}
16	1180	1062	1923		880 710			
18	1132	701	1599		563 999			
20	1028	868	1157	501	1326			
22	928	858	1644	746	1103			

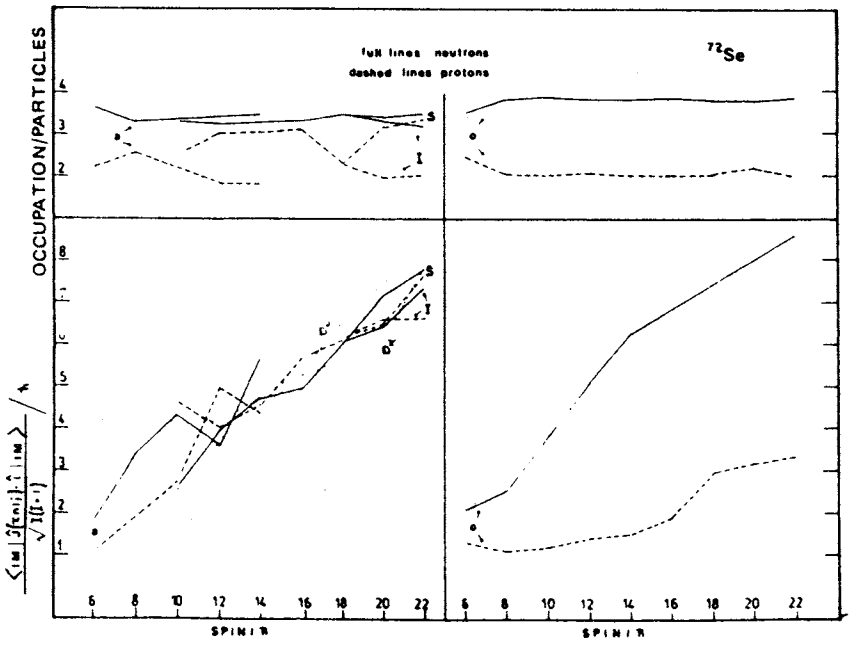

Fig.16. Same as in Fig.13, but for ^{72}Se, using again full lines for neutrons and dashed lines for protons. The labels of the bands are the same as in Fig.10.

possible that the experimental yrast band seen to high spins is a composite of several bands all with quite large deformation and linked by a very fast $E2$ path. In Table 3 we give for comparison the experimental $B(E2)$ values reported by different groups [40,45,46]. The experimental trend observed in the $B(E2)$ values could be reproduced by a theoretical composite path consisting of high spins from the S-band states which feeds by strong $M1$, $\Delta I = 0$ transition the yrast band at spin 10^+. Large $B(E2)$ values above spin 10 indicate the oblate band as a possible competing band, too. One needs more lifetime measurements to test this prediction.

The analysis of the wave functions reveals a variable mixing of more or less deformed prolate mean fields. The fastest decaying bands are strongly deformed quadrupole bands (labelled S and D in Fig.10). Again strong $M1$, $\Delta I = 0$ transitions connecting medium spin states have been found.

Figure 16 displays the neutron and proton alignments for the $g_{9/2}$ spherical orbital in the above labelled bands. No sharp alignment can be seen. This microscopic picture explains the missing backbending inferred from the experimental spectrum of ^{72}Se. The neutrons and protons bring almost the

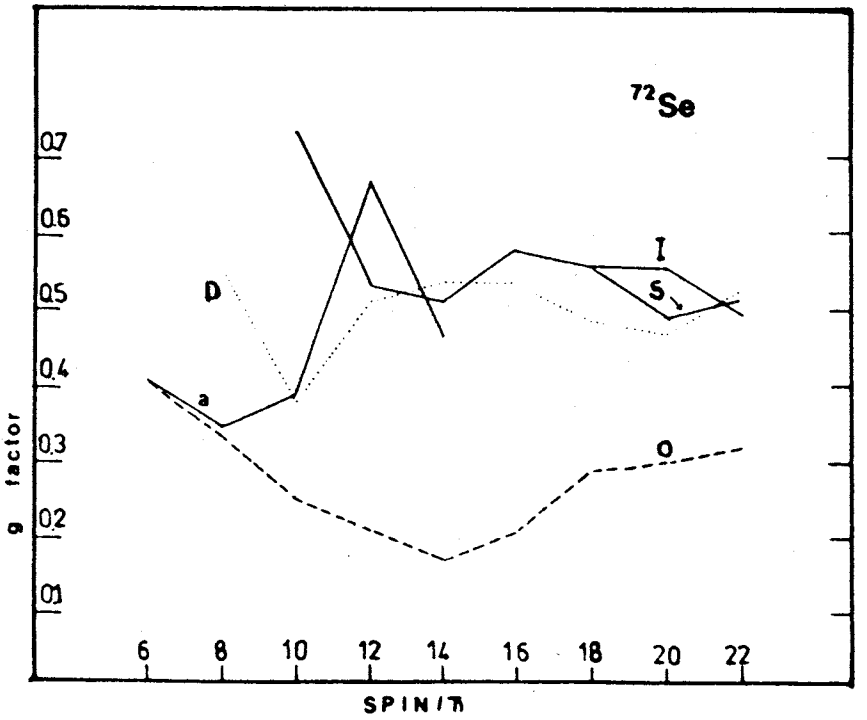

Fig.17. Same as in Fig.14, but for ^{72}Se

same contributions to the total angular momentum in all bands except for the oblate band where the alignment for the two protons is as expected more difficult. In the upper part of Fig.16 we show for comparison the occupation numbers for protons and neutrons in the $g_{9/2}$ spherical orbit.

The alignment picture is directly reflected by the gyromagnetic factors given in Fig.17 for the a, S, I, D and oblate bands. Small g-factors characterize only the oblate states as it is suggested by the strong neutron and weak proton alignment displayed in Fig.16. Thus the g-factor values could be used in this case as a possible fingerprint of the oblate band. Free values for the neutron and proton spin g-factors were used throughout the calculations.

Since the experimental information on the high-spin states is far from being complete and the accuracy of the data is still rather poor, we think that our theoretical results and also the conclusions emerging from the calculations of the side feeding times in this mass region [40] open many questions and ask for the continuation of the experimental investigations of the nucleus ^{72}Se.

3.3. Discussion. Summarizing the results obtained within the *real* EXCITED VAMPIR approximation concerning the structure of the positive parity low- and high-spin states of even-even nuclei in the $A \sim 70$ mass region we may conclude that many types of shape coexistence have been found. Our interpretation strongly supports the shape coexistence as a dominant feature of the low spin states. This persists and manifests specifically at high spin states. We predicted a strong bunching of states of a given spin in small excitation energy interval and a variable, sometimes very strong, mixing in between these states which creates a complex feeding pattern for the yrast band including competing $M1$, $\Delta I = 0$ transitions. Nevertheless, the high spin states can still be grouped into multiple bands based on different structures, some of them connected by $E2$ crossing transitions.

This complex behaviour was delivered by an approximation which, at least in principle, can describe excitations of arbitrary complexity, and by its chain of variational calculation automatically selects the relevant degrees of freedom for each particular state under consideration irrespective of whether they are of collective or single particle nature.Furthermore,by construction this approach minimizes the residual interaction between its different solutions and hence successively creates an optimal A-nucleon basis for a given symmetry. Thus it is expected that already with a small number of configurations an excellent description of the structure of the investigated states can be reached.

Now, concerning the comparison of our results for the $A \sim 70$ mass region with the experimental information, qualitatively, the overall agreement with the available data is not bad, quantitatively, however, especially as far as the $B(E2)$ values are concerned, still many discrepancies and open problems appeared. Since experimentally the side feeding times in this mass region are not yet firmly handled [40], the measured $B(E2)$ values reported by different groups are too spread and the available data concerning other observables were too scarce, we saw no reason to change the renormalization of the effective Hamiltonian. Obviously changes in this renormalization as well as the inclusion of additional correlations were supposed to alter the quantitative results obtained within the *real* EXCITED VAMPIR approximation. However, concerning the qualitative features as, for example, the coexistence of many differently deformed structures and the resulting high level density even for the high-spin values, one would expect to survive such improvements of the theoretical description. What we have obtained proceeding on these lines to get improvements and tests of our achievements will be described in the next section.

4. NEW ASPECTS OF THE NUCLEAR-SHAPE COEXISTENCE VIA THE *REAL* EXCITED FED VAMPIR APPROACH

Being restricted to always only one additional determinant for each new state with the considered symmetry, the EXCITED VAMPIR approach is, however, essentially a mean-field approximation. The residual interaction between the lowest few configurations for each symmetry may not be the dominant one for the lowest states especially in regions with a high level density as it is encountered in the $A \sim 70$ mass region. The EXCITED FED VAMPIR approximation which allows one to include the dominant correlations for each particular configuration irrespective of their excitation energy in a systematic way using again variational procedures has the advantage that the residual interaction between the correlated states becomes much smaller than in the case of the uncorrelated EXCITED VAMPIR solutions and thus increases the reliability of the wave functions considerably. In the following we shall demonstrate that the qualitative features of the complex behaviour of the nuclei in the $A \sim 70$ region obtained within the less sophisticaled EXCITED VAMPIR procedure do persist, however, quantitatively new aspects could be obtained.

4.1. Charge and Transition Charge Densities in Some Even Mass Ge Isotopes. Based on the assumptions given in section (2.1) the effective Hamiltonian for all the considered nuclei was built as it is explained in section (3.1). Then correlated *real* EXCITED FED VAMPIR wave functions for the lowest two $I^\pi = 0^+$ and 2^+ states have been calculated in two chains of isotopes: ^{68,70,72,74,76}Ge and ^{72,74,76}Kr. As described above, for each particular state first a single symmetry-projected configuration, being properly orthonormalized with respect to the correlated solutions for the energetically lower states with the same symmetry, was used as test wave function. The resulting «dominant mean field configuration» had been then correlated by successively adding further determinants and determining the underlying mean fields again by variation. In this procedure the energy gains due to subsequently added configurations do decrease by construction and the chain of variational calculations has been truncated as soon as these gains became of the order of about 100 keV. The resulting numbers of symmetry-projected quasiparticle determinants used for each state varied from 4 to 6 for the 0^+ ground states and from 4 to 5 for the first excited 0^+ levels. For angular momentum 2^+ the corresponding numbers were 3 to 5 for the first and 2 to 4 for the second state, respectively. Finally, the residual interaction in between the correlated solutions for the same symmetry has been diagonalized.

A similar picture to the *real* EXCITED VAMPIR one emerged from the *real* EXCITED FED VAMPIR studies on the structure of low-spin states in

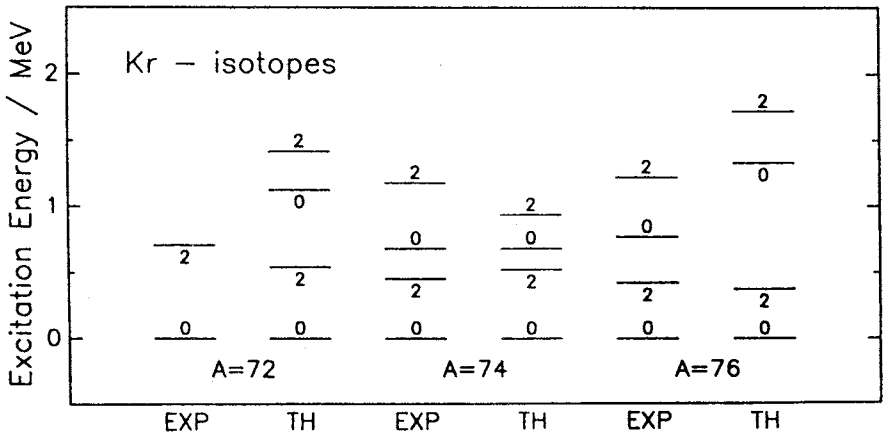

Fig.18. The excitation energies of the first excited 0^+ states as well as of the lowest 2^+ states obtained within the *real* EXCITED FED VAMPIR approach for the isotopes ^{72,74,76}Kr are compared to the experimental data

the investigated chains of Kr and Ge isotopes. In Fig.18 the excitation energies for the calculated $I^\pi = 0^+$ and 2^+ states in the ^{72,74,76}Kr nuclei are compared with the available experimental data. As can be seen the agreement is fairly good, especially for a completely microscopic calculation. The structure of the lowest two 0^+ and 2^+ states in the Kr isotopes is dominated by oblate-prolate shape coexistence.

In a next step we have tried to confirm rather a complicated picture emerging from the REV and REFV approaches for the structure of nuclei in the $A \sim 70$ mass region on a more quantitative basis. For this purpose we have calculated the charge densities for the first two $I^\pi = 2^+$ states in several even Ge isotopes [18] and compared the results with the data extracted from elastic and inelastic electron scattering [19].

The wave functions resulting from any of the approaches presented in section (2.2) are quantum mechanical many particle states having proper symmetry quantum numbers and can thus be used to calculate various observables. In order to obtain the transition charge density in between two REFV solutions $|\Psi_i>$ and $|\Psi_f>$ for a particular nucleus, e.g., we have to calculate the matrix elements of the charge density operator

$$\hat{\rho}_{ch}(\mathbf{r}) = \frac{1}{(2\pi)^3} \int d^3\mathbf{q} \exp\{i\mathbf{q}\cdot\mathbf{r}\} f_{CM}(q) f_p(q) \sum_{i=1}^{A} e_{\tau_i} \exp\{-i\mathbf{q}\cdot\mathbf{r}_i\} \qquad (4.1)$$

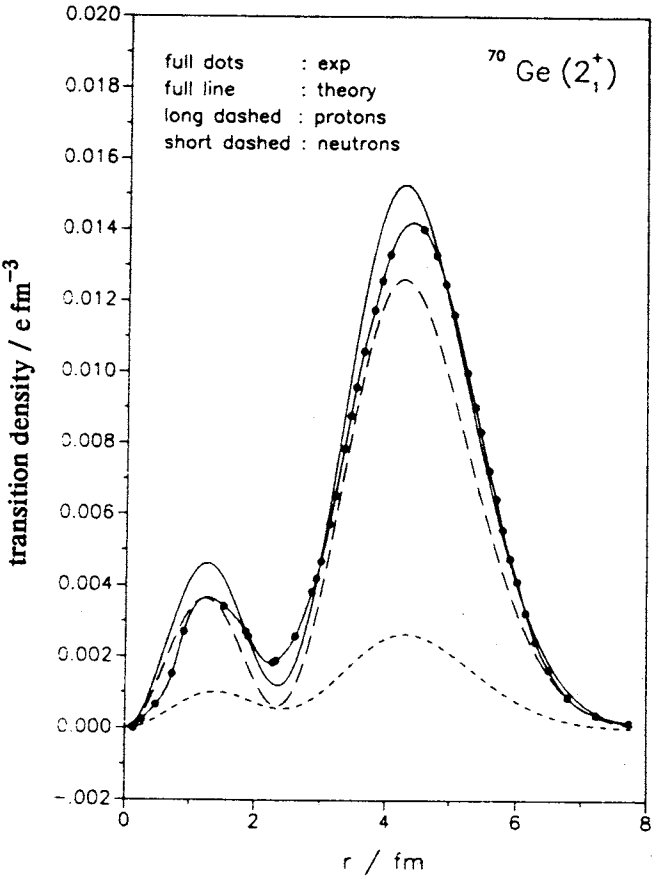

Fig.19. The calculated transition charge density for the 2_1^+ state in ^{70}Ge is compared to the experimental data out of ref.[19]. The total theoretical transition density is furthermore decomposed into its proton and neutron components. Effective charges of $e_n = 0.17$ and $e_p = 1.17$ have been used

between these two states. Here e_{τ_i} denotes the effective charge of the proton or neutron i and the Gaussian

$$f_p \equiv \exp\left\{-\left(\frac{aq}{2}\right)^2\right\} \tag{4.2}$$

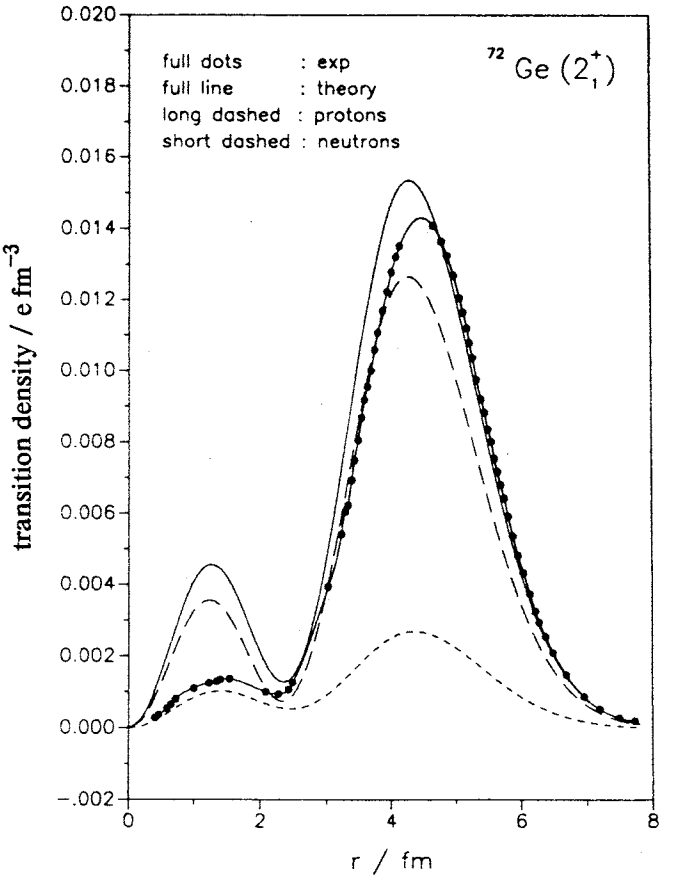

Fig.20. Same as in Fig.19, but for the 2_1^+ state in ^{72}Ge

with a width parameter of $a = 0.656$ fm approximates the charge distribution of a single proton [47]. The usual Trassie — Barker factor [48]

$$f_{CM} \equiv \exp\left\{\frac{1}{A}\left(\frac{bq}{2}\right)^2\right\} \tag{4.3}$$

was introduced to correct the violation of the translational invariance in both the operators as well as in the wave functions (b is the oscillator length parameter used for the single particle basis wave functions). This correction factor is completely sufficient here for the approximate treatment of the center

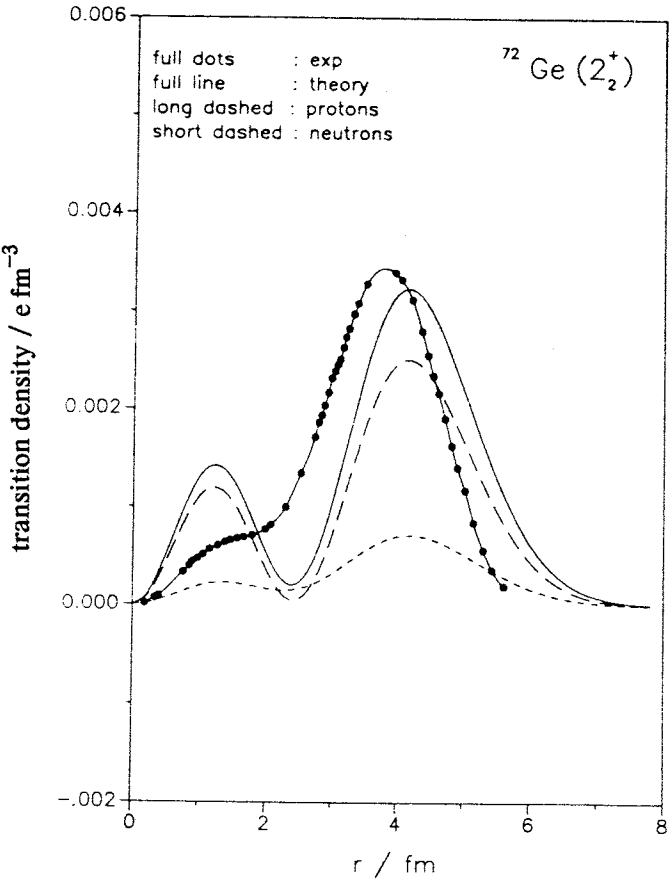

Fig.21. Same as in Fig.19, but for the 2_2^+ state in ^{72}Ge

of mass motion, because of the relatively large mass of the nuclei considered, and since furthermore a pure harmonic oscillator single particle basis is used.

The theoretical description of the spectra and electromagnetic transition probabilities which were illustrated above is also supported by the results [18] for the charge transition densities from the ground to the first and second 2^+ levels in several Ge usotopes. To exemplify we compare the calculated charge transition density to the collective 2_1^+ state in ^{70}Ge and ^{72}Ge with the experimental results [19] from inelastic electron scattering in Figs.19 and 20, respectively. As can be seen the agreement is excellent. For ^{74}Ge and ^{76}Ge, however, the magnitude of the experimental transition density is consider-

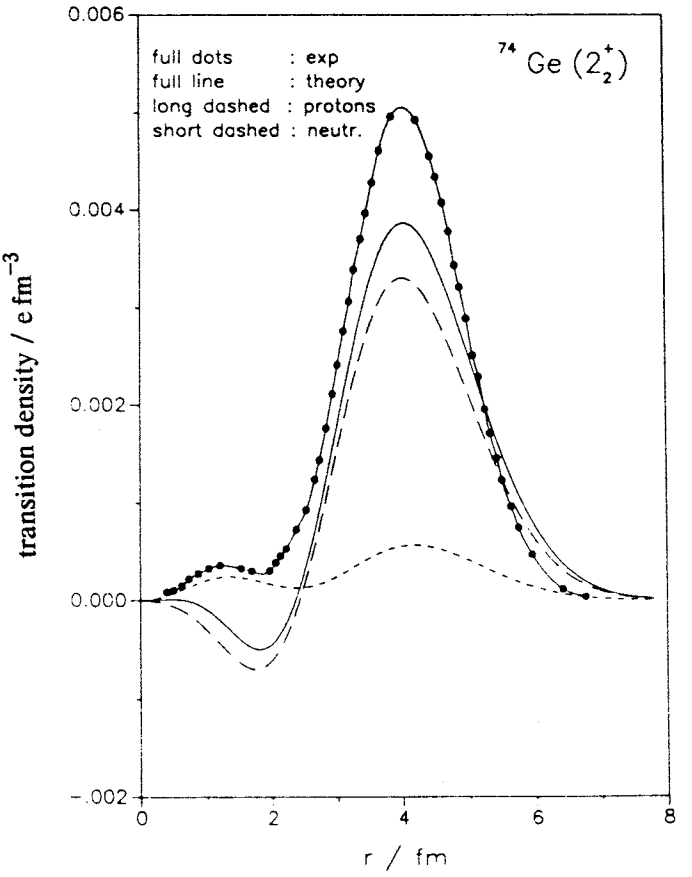

Fig.22. Same as in Fig.19, but for the 2_2^+ state in ^{74}Ge

ably understimated though the shape is in both cases reasonably well reproduced by the calculations. It should be mentioned that here no adjustment of the effective charges (0.17 for neutrons and 1.17 for protons) used in the REFV calculations to investigate other electromagnetic properties of the considered nuclei has been done. The transition charge densities for the much smaller noncollective transitions to the second 2^+ states are obviously even more sensitive. However, here too, the shapes of the calculated densities are in reasonable agreement with the experiment (with the exception of the small negative hump at small radii in ^{74}Ge) and also the magnitude of the densities could be reproduced, as can be seen from Figs.21 and 22. In these

figures the transition charge densities obtained for the noncollective 2_2^+ transitions in ^{72}Ge and ^{74}Ge, respectively, are compared with the available experimental data. In ^{76}Ge again the shape of the experimental transition charge density is reasonably well reproduced while the magnitude is drastically underestimated.

Both the 2_1^+ as well as 2_2^+ transitions are better reproduced in the present calculations than in the Skyrme — Hartree — Fock — Bogolubov calculations of Girod, Gogny and Grammaticos [49] being discussed also in ref. [19]. The improvement obtained by the present symmetry-projected few determinant calculations with respect to the one determinant Skyrme-HFB description is a strong indication that the mixing of configurations corresponding to different shapes which is obtained as the prominent feature of the structure of the low spin states of the nuclei in this mass region in our completely microscopic variational calculations does play an important role at least in the doubly-even Ge, Se and Kr isotopes.

4.2. Some New Aspects of the Shape Coexistence in the Nucleus ^{68}Ge. Using the same model space and the same effective Hamiltonian as in the *real* EXCITED VAMPIR approximation we reinvestigated the spectrum of ^{68}Ge with the *real* EXCITED FED VAMPIR procedure, not without some hesitation, since our earlier more restricted description of this nucleus got some at least qualitative support from new experimental data [17]. Fortunately, however, as we shall see, the qualitative features of the earlier description do persist.

We have constructed correlated REFV wave functions for three lowest 0^+, 2^+ and 4^+, four lowest 6^+, five lowest 8^+, 10^+, 12^+ and 14^+, six lowest 16^+ and seven lowest 18^+ levels of ^{68}Ge. As it was already mentioned, first the «main mean field» is obtained and then the «correlating configurations» for each state of a given symmetry. The additional correlations have been kept in the variational chain as far as the energy gain was still of the order of 100 keV. The resulting numbers of symmetry-projected quasiparticle determinants used for each state varied from 1 to 7. After the diagonalization of the residual interaction, here much smaller than in the REV approach, the solutions have been grouped into several bands entirely according to the $B(E2)$ transitions in between them. The new theoretical spectrum together with the new experimental results are given in Fig.23. Since neither the model space, nor the effective interaction have been changed, the results can be directly compared to that one obtained within the more restricted EXCITED VAMPIR approach.

In comparing the EXCITED FED VAMPIR spectrum (left side of Fig.23) with the EXCITED VAMPIR one (left side of Fig.8) it becomes obvious that the essential qualitative features of the calculated spectrum like, e.g., the

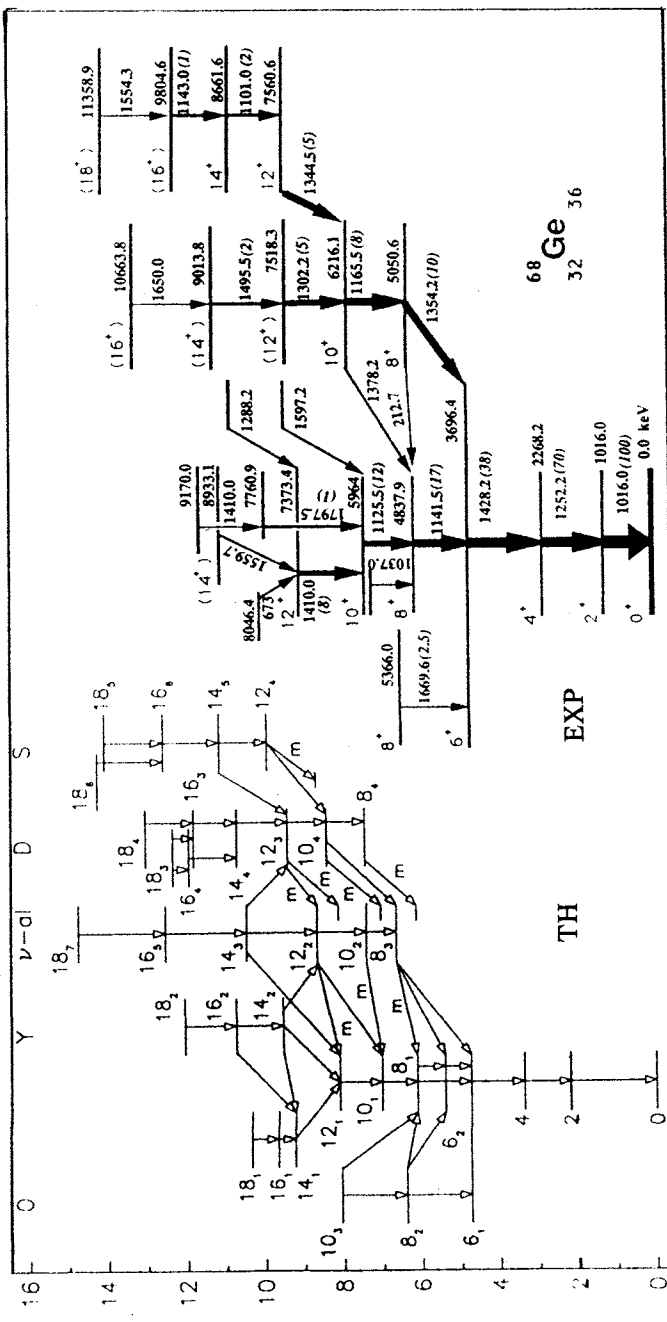

Fig.23. Positive-parity levels in ^{68}Ge nucleus. The theoretical spectrum as obtained in the *real* EXCITED FED VAMPIR approach (left side) is compared to the recent experimental results (right side). The symbols used to identify the calculated bands are described in the text. The experimental bands are ordered (oblate on the left, superdeformed on the right) to match up with the calculated levels on the left side and matching the observed properties (lifetimes, magnetic moments, and moments of inertia) of each band with the calculated properties of each band. The *D*-band in the calculations may be the new band which feeds the 5963 keV 10^+ level (ref. [17])

Table 4. The amount of correlations and the corresponding energy gains as obtained within the *real* EXCITED FED VAMPIR approach for some selected states of the nucleus ^{68}Ge *before* the residual interaction in between the various solutions for each considered symmetry is diagonalized

I_i [ħ]	n_c	$\|\psi_c\|^2$ [%]	E_c [keV]	I_i [ħ]	n_c	$\|\psi_c\|^2$ [%]	E_c [keV]
0_1	4	6	1221	12_1	4	27	681
2_1	6	14	637	12_2	3	14	409
2_2	4	14	502	16_1	3	14	685
2_3	2	20	708	16_2	4	14	842
8_1	2	2	226	18_1	3	9	596
8_2	4	12	502	18_2	2	17	668
8_3	5	24	767	18_3	1	14	605
10_1	4	16	550				
10_2	4	8	521				
10_3	2	4	274				

The first column presents the angular momentum with a subscript referring to the position of the state in the spectrum. In the next column the number of correlating configurations being used on top of the dominant mean field configuration for this particular state is presented. The amount of correlations $|\psi_c|^2$ they contribute with respect to the latter is given in the next column and, finally, the corresponding correlation energy is presented. Note that this numbers refer to the already *orthonormalized* solutions

occurrence of many coexisting bands at comparable excitation energies and the complexity of the resulting decay pattern, are not influenced by the additional correlations. Furthermore all the various bands obtained in the earlier calculations do occur in the improved approach, too. This can be seen, e.g., from Table 5 which compares the spectroscopic quadrupole moments and $B(E2)$ values of these bands as obtained in the REFV approach with those resulting from the REV uncorrelated calculations. Except for some discrepancies at angular momentum 8^+ and 14^+ the agreement is very good. Furthermore the fact that in both calculations essentially the same structures are obtained is supported by the amount of angular momentum which the

Table 5. The spectroscopic quadrupole moments Q_2^{sp} (in $e\cdot\mathrm{fm}^2$) and the $B(E2; I \to I-2)$ (in $e^2\mathrm{fm}^4$) values for some of the theoretical bands obtained for the nucleus ^{68}Ge

	Q_2^{sp} [$e\cdot\mathrm{fm}^2$]							
I[$\hbar$]	Y		$\nu - al$		D		S	
	REFV	REV	REFV	REV	REFV	REV	REFV	REV
2	28	29						
4	49	48						
6	55	53	−72	−68				
8	−56	−40	−62	−71	−102	−87	−102	−77
10	−75	−79	−65	−59	−107	−106	−107	−102
12	−81	−78	−66	−68	−92	−103	−108	−99
14	−83	−85	−53	−54	−98	−104	−120	−110
16	−86	−86	−53	−55	−97	−96	−118	−117
18	−85	−89	−45	−46	−96	−93	−103	−101

	$B(E2; I \to I-2)$ [$e^2\mathrm{fm}^4$]							
I[$\hbar$]	Y		$\nu - al$		D		S	
	REFV	REV	REFV	REV	REFV	REV	REFV	REV
2	100	181						
4	563	633						
6	792	834						
8	291	503						
10	852	798	677	500	1870	1367		
12	854	919	619	561	1234	1259	733	1549
14	273	332	285	206	856	1207	1732	1449
16	672	960	388	349	1137	997	2163	1390
18	921	907	325	237	837	708	1445	1148

Compared are the results of the *real* EXCITED FED VAMPIR (REFV) calculations (Fig.23) and those of the more restricted *real* EXCITED VAMPIR (REV) approach (Fig.8). In both cases effective charges of $e_n = 0.25$ and $e_p = 1.25$ have been used. The labels referring to various bands are explained in the text

valence protons and neutrons in the $0g_{9/2}$ shell-model orbit contribute to the total spin in various bands. A comparison of the alignment plots is given in Fig.24. As can be seen the inclusion of the additional correlations by REFV causes again no essential qualitative modifications with respect to the REV results. Since, last but not least, also the transition energies within various bands were in most cases not very much affected, we may conclude that at least as far as the qualitative features are concerned our REV description of this nucleus was essentially confirmed by the more sophisticated REFV procedure.

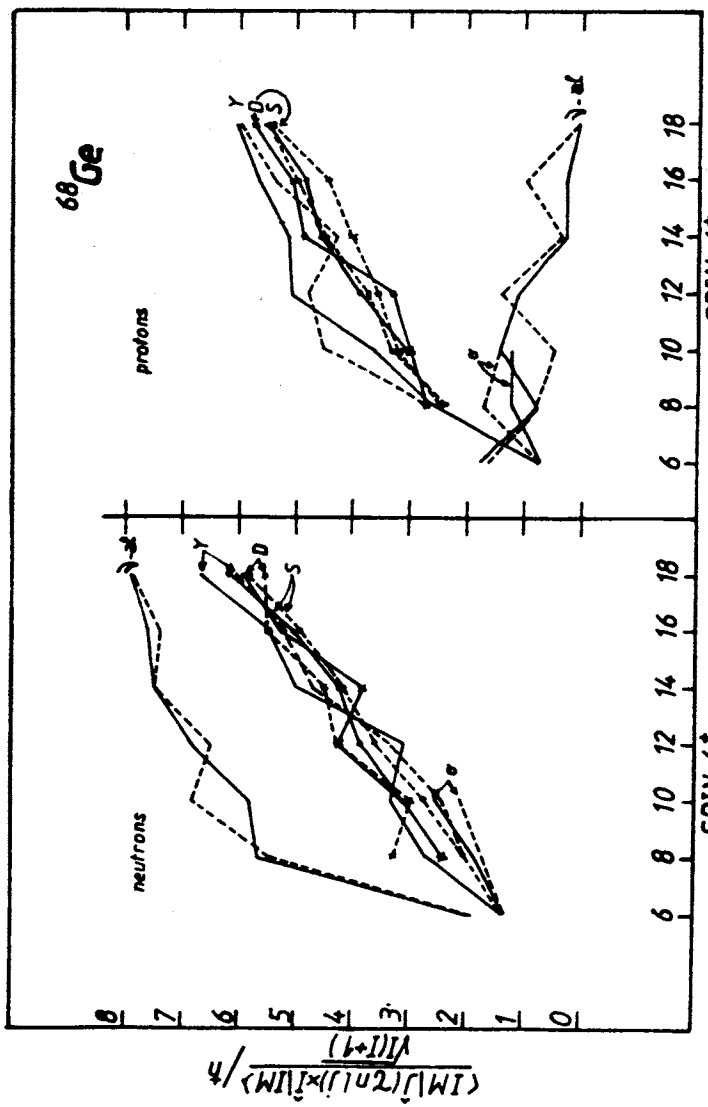

Fig. 24. The neutron (left side) and proton (right side) alignments of the $0g_{9/2}$-shell model orbit for the nucleus ^{68}Ge. The full lines refer to the results of the correlated *real* EXCITED FED VAMPIR approach; the dashed ones to those of the more restricted *real* EXCITED VAMPIR calculations

Concerning quantitative details, however, the two approaches display some distinct differences. Comparing, e.g., the energy of the correlated few-determinant solution (before the diagonalization of the residual interaction) with that of the dominant first configuration, being created for each state, one obtains in most cases energy gains which are comparable with the level spacings and thus considerable. Table 4 displays these «correlation-energies» as well as the corresponding deviations of the correlated from the dominant «one-configuration» wave functions for a couple of selected states. As can be seen, the correlation energies which are in average of the order of about half a MeV display, however, some variations with angular momentum as well as excitation energy. The corresponding deviations from the dominant component in the wave function vary in between almost nothing and about 30%. Note, that the states being selected here are typical examples. For all the other levels out of Fig.23 similar results have been found.

The most drastic effect is obtained for the 0^+ ground-state: altogether about 6% of correlations, but 1221 keV of additional binding for the REFV solution which is about half a MeV more than any energy gain found for the higher spin states. Consequently the $2_1^+ \rightarrow 0_1^+$ transition energy becomes now considerably larger than observed experimentally. This discrepancy has essentially two reasons, first, to make a comparison between REV and REFV results we used the renormalizing corrections to the nuclear matter *G*-matrix adjusted within the EXCITED VAMPIR approximation and not within the more general few determinant approach. Second, even in the REFV approximation the underlying mean fields are still considerably «symmetry-restricted» and we shall see in the next section what improvement the introduction of «complex» HFB mean field does. Keeping this deficiency in mind we shall compare the REFV results with the new experimental data [17] for the high-spin positive-parity bands in the nucleus ^{68}Ge by renormalizing the theoretical spectrum to the corresponding 2_1^+ level.

Up to angular momentum 6^+ the calculated yrast levels are almost pure oblate states. The oblate band (*O* in Fig.23) then continues with the second 8^+ (about 85% oblate) which most probably has to be associated with the experimental 8_3^+ and as in the REV approximation starting with 10_3^+ these oblate states are almost pure but at rather high excitation energy and therefore probably only weakly populated. Besides this oblate structure four other pronounced bands are obtained in the calculations. They are all prolate deformed but differ in the magnitude of their quadrupole and hexadecapole moments as well as in their pairing properties and display different alignments, too.

As in REV calculations the band labelled as $\nu - al$ is characterized by an almost empty $0g_{9/2}$ proton level while the neutrons in the same shell-model orbit contribute here a conciderable portion of the total angular momentum. This strong neutron alignment is reflected in the small g-factors of the members of this band with again a small negative value for the 8_3^+ as in REV approach and in the data for the experimental 8_2^+.

The two bands labelled as D and S have almost the same quadrupole deformation on the neutron side, however, on the proton side the latter band is considerably more deformed. This is evident from the intrinsic quadrupole moments ($\beta_2 \cong 0.42$ as compared to $\cong 0.34$) of the leading configuration as well as from the $B(E2)$ values which above spin 12^+ are about twice as large in the S than in the D band. It should be stressed that in the recent experimental data one of the new bands has a large momentum of inertia than the previously known ones. In fact as can be seen comparing the old data (Fig.8) and the new ones (Fig.23) the three known bands beginning at 8^+ are found to exibit crossing transitions and other new bands are discovered to feed into them. It is remarkable that the complex band structure predicted by the calculations (REV as well as REFV) is supported by a similar picture revealed by the new experimental evidence.

All the calculated prolate bands have one common feature: their members become strongly mixed as soon as spin values as low as 14^+ or 12^+ are reached. Consequently, there are many competing decay branches for the various 14^+, 12^+, 10^+ and even 8^+ states. Thus the decay does not only run via streched $E2$'s within the various bands but also via some rather strong $B(E2)$'s for $\Delta I = 2$ as well as a couple of strong $\Delta I = 0$, $M1$ transitions (indicated by m in the figure) mainly feeding the yrast band (Y) at these angular momenta. So, e.g., the calculated 8_1^+ is linked to the 8_3^+ and the 8_4^+ by B(M1) values of 1.94 and 0.46, the 10_1^+ to the 10_2^+ and the 10_4^+ by even 4.21 and 0.47, and the 12_1^+ to the 12_2^+ and 12_3^+ by 0.82 and 0.64 (all in μ_N^2), respectively. Such crossing transitions are seen in the new experimental data, too. The resulting complex decay pattern may explain at least some of the irregularities seen in the experimental data, and obviously the theoretical results are strongly supported by the observation of not only several 8^+ but also several energetically bunched 10^+, 12^+ and 14^+ states.

Concerning the $B(E2)$ values, it is expected that uncertainties in the feeding times in such complex decay patterns as observed in ^{68}Ge nucleus could lead to considerable errors and from here may be the large error bars and still disagreement in the data from several experiments [34, 37—39].

Thus the comparison with the data needs a lot of further investigation. As can be seen from Table 5 the EXCITED FED VAMPIR approach yields for the $B(E2)$'s rather similar results as the more restricted EXCITED VAMPIR approximation and thus in this respect the inclusion of the additional correlations yields no new aspects.

4.3. Discussion. We have tried to test our microscopical description of the complex behaviour of the nuclei belonging to the $A \sim 70$ mass region using the more sophisticated *real* EXCITED FED VAMPIR approach. These studies confirmed rather a complicated picture emerging from the *real* EXCITED VAMPIR approximation for the considered nuclei.

Increasing the reliability of the resulting wave functions considerably by introducing additional correlations on the top of the symmetry-projected quasiparticle mean fields we reinvestigated the ^{68}Ge nucleus. It turned out that the essential qualitative features of the REV results concerning the complexity of the decay pattern, the competition of various configurations corresponding to different *shapes*, etc., and even the structure of the various bands were not influenced by the additional correlations brought in by the REFV procedure. Even more, the new ^{68}Ge data [17] are in striking agreement with the complex band structures and multiple shape coexistence predicted for ^{68}Ge including the band-crossing transitions and the new band with superdeformation. Quantitatively, however, a couple of changes was obtained which, in particular, support the need for some modifications of the effective Hamiltonian which before had been adjusted only within the more restricted *real* EXCITED VAMPIR approach.

Trying to confirm the complicated REFV picture for ^{68}Ge on a more quantitative basis we have calculated the charge densities for the ground states and the transition charge densities for the first two $I^{\pi} = 2^{+}$ states in several even Ge isotopes and compared the results with the data extracted from elastic electron scattering In the lighter nuclei ^{70,72}Ge the calculated densities are in good agreement with experiment. In the two heavier nuclei ^{74,76}Ge on the other hand the calculations miss a considerable part of the collectivity observed experimentally. This defect is a strong indication that either the renormalization of the effective Hamiltonian performed up to now is not sufficient or instead of the purely real HFB transformations being used here the essentially complex ones should be admitted or both. In the next section we shall introduce the essentially complex HFB transformations which allow one to account for time-odd correlations in the underlying mean fields in order to learn something more about the effective two-body interaction and how does it perform in a given model space.

5. COMPLEX MEAN FIELDS

The results obtained within the real VAMPIR approaches for the $A \sim 70$ mass region indicated a variable oblate-prolate mixing and a shape transition from oblate to prolate deformed shapes with increasing A. As for $N = Z$ nuclei both neutrons and protons are simultaneously filling the same levels and the neutron-proton interactions are significant, one expects that the shell stabilized shapes should be particularly bound and also a direct connection can be made between the *shape* of such a nucleus and its underlying nuclear structure. On the other hand the description of the structure of these nuclei is a sensitive test for the theoretical models. The most sophisticated VAMPIR models going beyond mean-field approximations are dealing with *complex* mean fields. The use of essentially *complex* HFB transformations allows for mixing of proton and neutron basis states as well as for parity mixing, providing a possibility of accounting for time-odd unnatural parity two-nucleon correlations while keeping time-reversal and axial symmetry. In this section we present the picture for the shape coexistence phenomena encountered in the $N = Z$, ^{72}Kr nucleus, emerging from the VAMPIR approaches based on *complex* mean fields. A comparison with the *real* calculations for the same model space and effective Hamiltonian is also given.

Using the «truncated» single particle basis and the effective two-body force presented in section 2.3 we constructed the *complex* EXCITED FED VAMPIR wave functions for the first two 0^+ and 2^+ states and the *complex* FED VAMPIR solutions for the yrast 4^+, 6^+ and 8^+ states in ^{72}Kr nucleus. The linear combinations of symmetry-projected determinants constructed for a state of a given symmetry contained two to five configurations. The energy gains introduced by the additional correlating configurations to each main component were succesively decreasing in any variational chain of calculations and these have been truncated as soon as the gains became of the order of 100 keV. The total energy gain brought to a state by the correlating configurations was decreasing with increasing spin as it was found already from the *real* calculations. But the same type of variational procedures applied for *real* HFB transformations in the same model space and using the same effective force led always to smaller energy gains from correlating configurations. A more suggestive parameter indicating the contribution of the additional correlations introduced already in the mean field by the *complex* HFB transformations is the total binding energy for the main configuration underlying the wave function of each calculated state. This supplementary energy varies between 1550 keV for the first 0^+ state and 1200 keV for the yrast 8^+ state and the first excited 0^+ state.

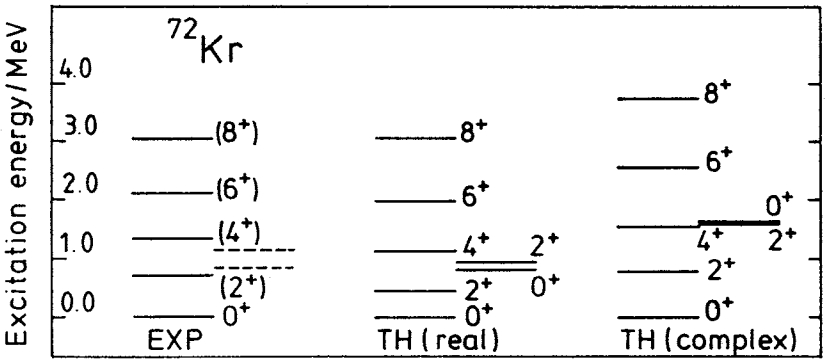

Fig.25. The theoretical spectrum as obtained within the FED VAMPIR or EXCITED FED VAMPIR approaches based on *complex* (most right) and *real* (middle) HFB transformations is compared to the recent experimental results [50,51] (most left) for the even spin positive parity states of the nucleus ^{72}Kr

In Fig.25 we compare the theoretical *complex* spectrum with the available experimental one [50, 51] for the investigated states in ^{72}Kr nucleus. Also the results obtained using only *real* mean fields are plotted. One can see from this figure that the experimental behaviour of the level spacing with increasing spin is well reproduced in the *complex* calculations. The main component in the wave functions for the yrast states is oblate deformed. The additional correlations introduced by the FED VAMPIR procedure brought energy gains of: 1094, 658, 602, 531 and 467 keV for 0^+, 2^+, 4^+, 6^+, 8^+ states, respectively. The main correlations came for the 0^+ ground state from a prolate deformed configuration which finally represents 34% in the wave function. The results indicate that from all additional configurations of CFV type for these states only one is prolate deformed. The contrubution of this component in the wave function is decreasing with the increasing spin: 7% for 2^+-, 3% for 4^+- and less than 2% for 6^+- and 8^+-state. The main component in the first excited 0^+ and 2^+ states is prolate deformed. The prolate-oblate mixing appears only in the wave function for the first excited 0^+ state, where the oblate component represents 16%. Even if the nature of the main components and of the additional correlating configurations are similar to those obtained in the *complex* calculations, the trend in the level spacing of the final spectrum is different for the *real* calculations and does not reproduce the experimental one equally well. The fact that the *complex* calculations reproduce the experimental trend in the level spacing is one of the improvements obtained introducing the neutron-proton interaction and the unnatural parity pairing

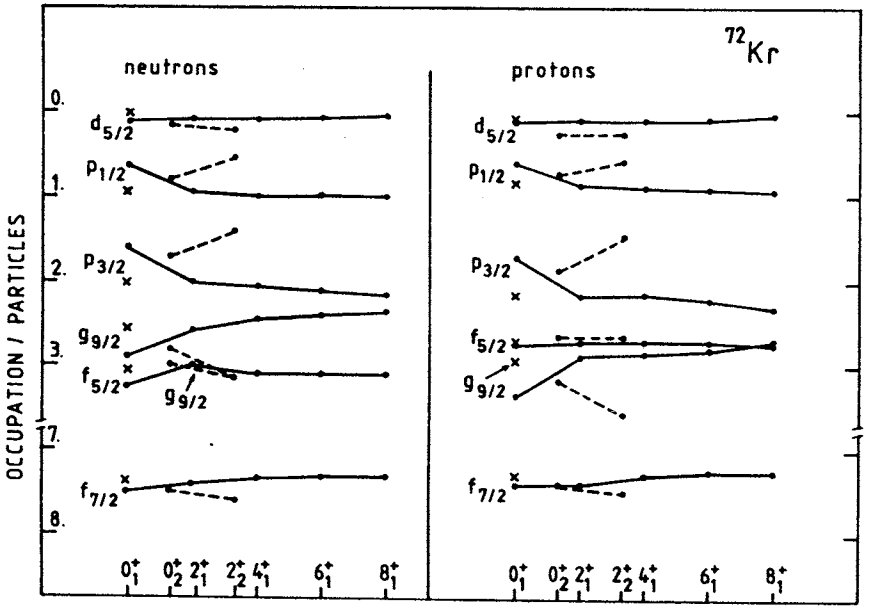

Fig.26. Neutron and proton occupation numbers of the spherical-basis orbitals for the lowest two 0^+ and 2^+ and for the yrast 4^+, 6^+, 8^+ states in ^{72}Kr. Full lines are for yrast states and dashed lines for the first excited states. The results have been calculated from the full wave functions, Eq. (2.24), based on *complex* HFB transformations. The crosses are for the one symmetry-projected determinant approximation to the 0^+ ground state

correlations (see Eq.2.19) in the HFB vacuum (Eq. 2.18). This seems to be essential for the $N = Z$, ^{72}Kr nucleus.

The intrinsic quadrupole moments of the building determinants of the wave functions for all the investigated states indicate almost identical contributions coming from the neutrons and from the protons. This is a strong indication that our effective force is well deviced and adequate to describe the complex structure of the nuclei belonging to this mass region. Other results obtained from our investigations within CFV or CEFV approximations give support to this conclusion. In Fig.26 are plotted the neutron and proton occupations for the spherical single particle orbits building the model space. Again the results indicate a very similar behaviour on the neutron and proton side. One can also observe a very smooth change with increasing spin. The 0^+ ground state has a special behaviour. By crosses are indicated the occupations for the main component of the corresponding wave function, which is oblate deformed, as for the other spin states. As can be seen it reveals similar

occupations to those coming from the full wave functions for the other spin states. The strong mixing of the mentioned prolate configuration produces the deviations observed in the occupations for the final linear combination calculated for this state. The prolate-oblate mixing only present in the first excited 0^+-, but not in 2^+-state, both containing a prolate deformed main determinant, is also reflected by the corresponding spherical occupations. Protons and neutrons have also similar contributions through $T = 1$ like-nucleon pairing correlations to the average pairing gap for all calculated configurations. In ^{72}Kr the contribution of the neutron-proton $T = 1$ pairing correlations to the total pairing energy varies from one configuration to another: it can be negligible, comparable, but also sometimes more important than the $T = 1$ like-nucleon pairing contribution. The results indicate a very small contribution coming from $T = 0$ neutron-proton pairing correlations.

It should be mentioned that our investigations using *complex* mean fields indicate that the main configuration for the first excited 4^+ and 6^+ states in ^{72}Kr are prolate deformed, as they appear also in the *real* calculations. Some preliminary studies on ^{74}Kr nucleus using *complex* HFB transformations show that the main configuration for the first 0^+, 2^+, 4^+ states is prolate deformed.

We can conclude that the prolate-oblate shape coexistence is also found in ^{72}Kr nucleus. A strong prolate-oblate mixing in the structure of the wave functions for a given state is obtained only for the first two 0^+ states and the yrast 2^+ state. The description of the structure of the $N = Z$, ^{72}Kr nucleus, which should mostly require for the introduction of the neutron-proton interaction in the mean field, is a sensitive test for both model and effective force.

6. CONCLUSIONS

In the present article some recent achievements concerning the microscopic description of the shape coexistence phenomena in the $A \sim 70$ mass region have been reviewed. The theoretical models involved in these investigations were the most sophisticated approaches belonging to the VAMPIR family, based on *real* and *complex* HFB transformations. The EXCITED VAMPIR model, being essentially a mean field approximation, and also the EXCITED FED VAMPIR method, going beyond mean fields, have been applied in a relatively large single particle basis, using realistic effective two-body forces, particularly designed to account for the complex structure of the nuclei belonging to the $A \sim 70$ region.

It was found that the shape coexistence phenomena dominate the structure of the investigated chains of even-even Ge, Se and Kr isotopes. The structure of these nuclei reveals both shape transition and shape coexistence. An oblate to prolate shape transition with increasing A emerged from the calculations. The structure of the low-spin states in the investigated nuclei, mainly 0^+ and 2^+ states, is dominated by a strong oblate-prolate mixing. A variable mixing of more or less deformed oblate and prolate symmetry-projected quasiparticle determinants is able to produce the experimental picture for the low spin states of the considered Ge and Se isotopes, like the presence of 4—5 coexisting 0^+ or 2^+ states in 3—4 MeV excitation energy, as well as the general trends observed for the quadrupole moments and electromagnetic transition probabilities, and proton and neutron occupations of the spherical single particle orbitals. It turned out from the investigation of the high spin states in some selected Ge and Se isotopes that the shape coexistence persists and manifests specifically at high spins. Our predictions concerning a strong bunching of states of a given medium or high spin and positive parity in a small excitation energy interval and a complex feeding pattern of the yrast line, including strong $M1$, $\Delta I = 0$ transitions for medium spin states were confirmed by recent experimental data in ^{68}Ge nucleus.

The recent studies concerning the structure of the $N = Z$, ^{72}Kr nucleus, based on *complex* HFB transformations, which allow one to include neutron-proton interactions and unnatural parity-pairing correlations in the mean field, revealed a good agreement between the theoretical results and the available data. This is also an indication that our effective force is rather well deviced for this mass region. A slightly, carefully readjusted renormalization of the effective two-body interaction is still needed, but it requires many more experimental data than available up to now, especially for the electromagnetic properties of the various states.

Even if a lot remains to be done, both theoretically as well as experimentally, the results presented here provide some interesting information on the way towards a more microscopic interpretation of the complex situation encountered in the nuclei of the $A \sim 70$ mass region.

ACKNOWLEDGEMENTS

The work presented here would have been impossible without the contribution of our collaborators: Frank Grümmer from Bochum, Esko Hammarén from Jyväskylä, Zheng Ren-Rong from Chonging, Mauro Kyotoku from João Pessoa. We are grateful to Profs. J.H.Hamilton and A.V.Ramayya for helpful discussions. One of us (A.P.) acknowledges partial

support from the Internationales Büro der KfK Karlsruhe, Germany, and the University of Jyväskylä and the Ministry of Trade and Industry, Finland.

REFERENCES

1. Hamilton J.H. — In: Treatise on Heavy-Ion Science, ed.D.A.Bromley; Plenum, New York, 1989, Vol.8, p.3.
2. Girod M., Grammaticos B. — Phys. Rev. Lett., 1978, 40, p.361.
3. Kumar K. — J. of Phys., 1978, G4, p.849.
4. Sakakura M., Shikata Y., Arima A., Sebe T. — Z. Phys., 1979, A289, p.163.
5. Didong M., Müther H., Goeke K., Amand Faessler. — Phys. Rev., 1976, C14, p.163.
6. Shikata Y., Sakakura M., Sebe T. — Z.Phys., 1981, A300, p.217.
7. Sakata F., Iwasaki S., Marumori T., Takada K. — Z. Phys., 1978, A286, p.195.
8. Weeks K.H., Tamura T., Udagawa T. — Phys. Rev., 1981, C24, p.703.
9. Takada K., Tazaki S. — Nucl. Phys., 1983, A395, p.165.
10. Petrovici A., Faessler A. — Nucl. Phys., 1983, A395, p.44.
11. Petrovici A., Faessler A., Köppel T. — Z. Phys., 1983, A314, p.227.
12. Schmid K.W., Grümmer F. — Rep. Prong. Phys., 1987, 50, p.731.
13. Petrovici A., Schmid K.W., Grümmer F., Faessler A., Horibata T. — Nucl. Phys., 1988, A483, p.317.
14. Petrovici A., Schmid K.W., Grümmer F., Faessler A. — Nucl. Phys., 1989, A504, p.277.
15. Schmid K.W., Zheng Ren-Rong, Grümmer F., Faessler A. — Nucl. Phys., 1989, A499, p.63.
16. Petrovici A., Schmid K.W., Grümmer F., Faessler A. — Nucl. Phys., 1990, A517, p.108.
17. Chaturvedi L., Zhao X., Ramayya A.V., Hamilton J.H., Kormicki J., Zhu S., Girit C., Xie H., Gao W.-B., Jiang Y.-R., Petrovici A., Schmid K.W., Faessler A., Johnson N.R., Baktash C., Lee I.Y., McGowan F.K., Halbert M.L., Riley M.A., McNeill J.H., Kortelahti M.O., Cole J.D., Piercey R.B., Jin H.Q. — Phys. Rev., 1991, C43, p.2541.
18. Petrovici A., Schmid K.W., Grümmer F., Faessler A. — Z. Phys., 1991, A339, p. 71.
19. Goutte D. — PhD-thesis, Universite de Paris-Sud 1984, Nr. d'ordre: ORSAY 2803.
20. Bloch C., Messiah A. — Nucl. Phys., 1962, 39, p.95.
21. Schmid K.W., Grümmer F., Faessler A. — Ann. Phys. (NY), 1987, 180, p.1.
22. Zheng Ren-Rong, Schmid K.W., Grümmer F., Faessler A. — Nucl. Phys., 1989, A494, p.214.
23. Petrovici A., Schmid K.W., Hammarén E., Grümmer F., Faessler A., to be published.
24. Holinde K., Erkelenz K., Alzetta R. — Nucl. Phys., 1972, A194, p.161.
25. Ring P., Schuck P. — The Nuclear Many-Body Problem, Springer, Berlin, 1980.
26. Rotbard G., La Rana G., Vergnes M., Berrier G., Kalifa J., Guibault F., Tamissier R. — Phys. Rev., 1978, C18, p.86.
27. Rotbard G., Vergnes M., Vernotte J., Berrier-Rousin G., Kalifa J., Tamisier R. — Nucl. Phys., 1983, A401, p.41.
28. Lecomte R., Kajrys G., Landsberger S., Paradis P., Monaro S. — Phys. Rev., 1982, C25, p.2812.
29. Mordechai S., Fortune H.T., Carchidi M., Gilman R. — Phys. Rev., 1984, C29, p.1699.
30. Vergnes M. — In: Proc. Int. Conf. on the Structure of Medium-Heavy Nuclei, Rhodos, 1979, Institute of Physics, Bristol, 1980, p.25.
31. Lecomte R., Irshad M., Landsberger S., Paradis P., Monaro S. — Phys. Rev., 1980, C22, p.1530.
32. Passoja A., Julin R., Kantele J., Luontama M., Vergnes M. — Nucl. Phys., 1985, A441, p.261.
33. Ramayya A.V., Ronningen R.M., Hamilton J.H., Pinkston W.T., Garcia-Bermudez G., Robinson R.L., Kim H.J., Carter H.K., Collins W.E. — Phys. Rev., 1975, C12, p.1360.

34. de Lima A.P., Ramayya A.V., Hamilton J.H., Van Noijen B., Ronningen R.M., Kawakami H., Piercey R.B., de Lima E., Robinson R.L., Kim H.J., Peker L.K., Rickey F.A., Popli R., Caffrey A.J., Wells J.C. — Phys. Rev., 1981, C23, p.213.
35. Heese J., Lieb K.P., Luhmann L., Raether F., Wöhrmann B., Alber D., Grawe J., Eberth J., Mylaeus T. — Z. Phys., 1986, A325, p.45.
36. Mylaeus T., Busch J., Eberth J., Liebchen M., Sefzig R., Skoda S., Teichert W., Wiosna M., von Brentano P., Schiffer K., Zell O., Ramayya A.V., Maier K.H., Grawe H., Kluge A., Nazarewicz W. — J. Phys., 1989, G15, p.L135.
37. Paradellis T., Kalfas C.A. — Phys. Rev., 1982, C25, p.350.
38. Morand C., Bruandet J.F., Giorni A., Tsan Ung Chan — J. de Phys., 1977, 38, p.1319.
39. Gusinskii G.M., Ivanov M.A., Lemberg I.Kh., Mishin A.S., Romanov V.S. — Izv. Akad. Nauk (ser. fiz.), 1977, 41, p.66;
Kiptilinyi V.G., Lemberg I.Kh., Mishin A.S. — Proc. Conf. on Nuclear Structure, Riga, 1979, Academy of Sciences, USSR, p.54.
40. Christancho F., Lieb K.P. — Nucl. Phys., 1988, A486, p.353.
41. Harada K. — Phys. Lett., 1964, 10, p.80.
42. Barclay M.E., Cleemann L., Ramayya A.V., Hamilton J.H., Maguire C.F., Ma W.C., Soundranayagam R., Zhao K., Balanda A., Cole J.D., Pircey R.B., Faessler A., Kuyucak S. — J. Phys., 1986, G12, p.12.
43. Frauendorf S. — Phys. Lett., 1981, B100, p.219.
44. Kemnitz P., Doring J., Funke L., Will E., Winter G. — Phys. Lett., 1983, B125, p.119.
45. Lieb K.P., Kolata J.J. — Phys. Rev., 1977, C15, p.939;
Hellmeister H.P., Schmidt E., Uhrmacher M., Rascher R., Lieb K.P., Pantelica D. — Phys. Rev., 1978, C17, p.2113.
46. Kiptilinyi V.G., Lemberg I.Kh., Mishin A.S., Pasternak A.A. — Bull. Akad. Sci. USSR, Phys. Ser., 1979, 43, p.26.
47. Elton L.R.B. — Nuclear Sizes, Oxford University Press, London 1961;
Willey R.S. — Nucl. Phys., 1963, 40, p.529.
48. Tassie L.J., Barker F.C. — Phys. Rev., 1958, 111, p.940.
49. Girod M., Gogny D., Grammaticos B. — In: 7ème Session d'Etude Biennale de Physique Nucleaire Aussois, 1983.
50. Varley B.J., Campbell M., Chishti A.A., Gelletly W., Goetting L., Lister C.J., James A.N., Skeppstedt O. — Phys. Lett., 1987, B194, p.463.
51. Dejbakhsh H., Cormier T.M., Zhao X., Ramayya A.V., Chaturvedi L., Zhu S., Kormicki J., Hamilton J.H., Satteson M., Lee I.Y., Baktash K., Mc.Gowan F.K., Johnson N.R., Cole J.D., Zganjar E.F. — Phys. Lett., 1990, B249, p.195.